Dynamics of surging glaciers in Svalbard and their potential in bed inference

Master thesis

Jonathan Kolar

Supervised by

Prof. Dr. Christian Haas and Prof. Dr. Andrew Hodson

University of Bremen

Germany

October 2024

Abstract

Recent studies show that the flow conditions during a glacial surge are exceptionally well suited for gaining information about basal topography. Here, an attempt is made to exploit these conditions and to asses the potential using surges in Svalbard for the first time. For this purpose, one of the globally most pronounced clusters of surging glaciers, located in Heer Land, south-eastern Spitsbergen, was studied between 2016 and 2024 using modern remote sensing data products. The result is an inventory and a characterization of a large variety of different surge and surge-like dynamics. Within the study area, surges, preceded by a pronounced bulge, slowly propagating bulges that never turn into a surge and frontal initiated tidewater surges without any bulges were all found side by side. These findings hint towards more complex mechanisms of surging than we currently can describe. Remotely sensed data from five of these surges, were used to apply a Bayesian bed inference approach. The model used in the inversion is based on the continuity equation evaluated along an one-dimensional flow line. It was found that the requirement of a nearly gap-free surface velocity time series presents the biggest constraint to this and future studies. Therefore, the data provided in the ITS_LIVE surface velocity product were carefully evaluated and tools to mitigate biased data are presented. The results confirm a significant improvement in model uncertainty with increasing ice velocities as they occur during a surge. For the cases with sufficiently good input data, the model was able to produce realistic bed topographies. However, the one-dimensionality of the applied model was found to limit the quality of the results in cases with more complex flow geometries.

Contents

1. Introduction

In the event of a glacial surge, a previously almost stagnant glacier experiences a dramatic speedup of orders of magnitude, leading to extreme velocities in the range of tens of meters per day (Meier & Post, 1969). Even if surging glaciers are rare in a global context, the existence of surges poses questions about glacial mechanics in general. Regarding the Earth's ice sheets, the importance of these mechanics becomes clear as there are ice streams with a surge like behavior which drain these ice reservoirs (Fowler and Johnson, 1996) and therefore play a major role in their stability. Therefore, it is remarkable that the process that causes surging is still not fully understood.

Kääb et al. (2023) identified Svalbard as one of the biggest global hotspot of currently active surges with an especially dense clustering in the area of Heer Land in south-eastern Spitsbergen (see Fig. 1.1). In a study, mainly focused on this cluster, the dynamics of Svalbard's surging glaciers were studied by Sund et al. (2009) from surface elevation change data. Based on this, an inventory of active surges and a three-stage concept for the evolution of a surge was established.

Today, more than a decade later, elevation data is available in high temporal resolution with accuracies improved by about an order of magnitude, compared to most of the products used by Sund et al. The availability of these high-resolution data inspires the first objective of this project of revisiting the Heer Land surge cluster by studying the current surface elevation change in the region.

The knowledge of the bed topography underlying a glacier is usually the starting point of every glaciological study and the boundary condition for any modeling. Further, uncertainty in ice thickness of all land ice is the number one error in estimations of future

Figure 1.1.: Satellite image (Sentinel-2, 2024-08-08) of the study area (Heer Land), south-eastern Spitsbergen, Svalbard. Selected glaciers are labeled and flowlines are indicated for the surging glaciers used for bed inference.

sea level rise. In recent years, three studies aimed at providing an ice-free topography of Svalbard (Fürst et al., 2018, Millan et al., 2022, van Pelt and Frank, 2024). Different approaches were chosen to use parameters observed at the glacier surface for the retrieval of bed topography. This included mass conservation based models, simple flow models and physics-informed ice flow models. All these approaches struggle in dealing with active surges, so that in the study of van Pelt and Frank surges were identified and treated with a heavily simplified perfect-plastic model. Despite these difficulties, Morin et al., 2023 were able to show in a pilot study that the high-slip flow during a surge can pose favorable conditions for bed inference studies. Based on the promising results of the latter study, the second objective of this study is to explicitly explore the potential of the numerous surges in Svalbard. For the retrieval of ice thickness and bed topography the continuity-based bed inference approach from Morin et al. (2023) will be applied. This shall be demonstrated for five surges in Heer Land.

In order to address these two objectives, remote sensing data which provide surface elevation change and surface velocity are used. In total, data extending from 2016 to 2024 from the region of Heer Land are assessed and used for bed inference.

2. Background: Surging glaciers

Traditionally, surge-type glaciers are defined by a cycle of quiescent and active phase driven by internal oscillations. During the active phase, the glacier experiences a dramatic increase in speed by one to two orders of magnitude compared to quiescence (Benn & Evans, 2013; Meier & Post, 1969). This implies that in both phases the glacier's mass balance is out of equilibrium. During quiescence, ice accumulates in the upper part while the glacier is thinning at the terminus. As the surge starts, mass is transported from the so called reservoir area to a receiving area at lower elevations. Such a behavior is illustrated in Figure 2.1. Maximum speeds differ from region to region but usually lay in the range of meters to tens of meters per day. Surging glaciers can reach such high velocities through a flow regime that is dominated by slippage between bed and glacier; internal deformation is of minor importance during a surge (Benn & Evans, 2013). Globally, only a small fraction (about 1 %) of all glaciers tend to surge (Sevestre & Benn, 2015). While most surge-type glaciers appear within an envelope of climatic conditions (Sevestre & Benn, 2015), a range of factors but no parameter alone seems to cause surge behavior. In all regions surging, glaciers tend to be longer and wider than their non-surging counterparts (Bouchayer et al., 2022; Clarke, 1991). Further, the underlying geology and surface slope have an impact on the probability of glaciers to be of surge-type (Jiskoot et al., 2000).

The purely internal nature of surge cycles was questioned as a consequence of surges observed to be spatially correlated and potentially initiated by meteorological influences (e.g., Eisen et al., 2001; Paul et al., 2022). Further, Kääb et al. (2018) described glacial collapses as a sudden appearance of surge-like behavior, emphasizing the importance

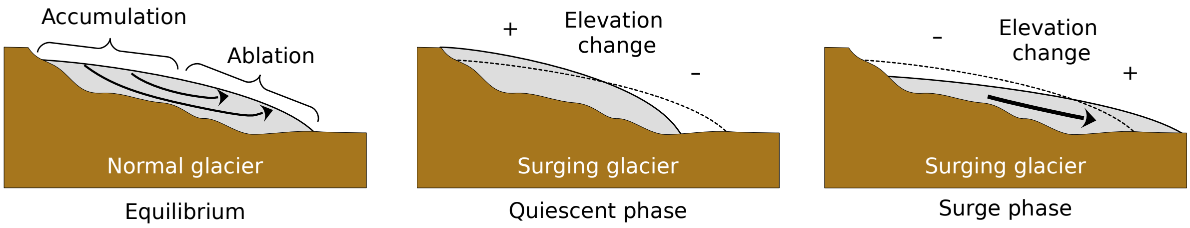

Figure 2.1.: Simplified concept of cyclic surging. For idealized, normal (non-surging) glaciers, mass balance and ice transport are in equilibrium and no surface elevation change takes place. Surging glaciers oscillate between quiescent and surge phase. During the quiescence, decreased motion leads to a steepening of the glacier surface. After the initiation of the shorter surge phase, the accumulated ice is transported downstream under increased velocities.

of non-cyclic surge models. Recently, an enhanced global clustering of active surges was found by Kääb et al. (2023), pointing further towards climatic influences on surge initiation.

2.1. Surge mechanism

A variety of mechanisms that lead to a cyclic instability of glaciers have been proposed. An exhaustive list of the different models can be found in Benn et al., 2019a. Two main ideas that aim at explaining surge behavior of temperate and polythermal glaciers shall be reviewed here briefly.

First, surge cycles on warm based glaciers seem to be caused by changes in the drainage system of the glacier. A feedback loop is caused as an effective, channelized drainage system is destroyed by the fast motion of a surge, leading to increased subglacial water pressure and decoupling of the glacier from its bed. This connection was proposed by Kamb et al. (1985) upon the observation of the 1982-1983 surge of Variegated Glacier, Alaska.

Second, thermal switching occurs on glaciers that are partially cold based (Clarke, 1976). Here a positive feedback loop (the thermal runaway) is created. The basal ice is warmed by frictional heating, which causes enhanced slipping between the glacier and its bed, leading to an increase in friction and stronger heating (Clarke et al., 1977). During the surge, a region of warm and fast ice develops at the top of the glacier and forms a surge bulge at the boundary with the cold and slow ice at the lower glacier. This bulge then travels downstream towards the terminus. Such a behavior was observed on multiple polythermal glaciers, e.g., by Hamilton (1992), Murray et al. (2000) and Frappé and Clarke (2007). However, Sevestre et al., 2015 showed in Svalbard that thermal switching alone is insufficient to explain surging.

The first general theory of a surge mechanism was proposed by Benn et al. (2019a) and combines heat and meltwater in the concept of enthalpy. It is argued that enthalpy and mass balance must be in balance continuously in order to allow a steady flow of ice. If that is not the case, oscillations occur in the form of quiescent and surge phase.

2.2. Evolution and classification

Sund et al. (2009) introduced a classification scheme of three consecutive surge stages based on a geodetic study in Svalbard. Stage 1 and 2 are marked by surface elevation change in the middle and upper glacier only. Typical is an initial lowering in the uppermost glacier, followed by a thickening further down. During this stage, velocities remain below those associated with an active surge phase. Therefore, no dramatic crevassing can be observed but surge bulges could occur. The line between stage 1 and 2 is drawn by the extent of the area with initial surface lowering. As this can be hard to quantify and might depend on observational precision, no differentiation between stage 1 and 2 is done in the following. Stage 3 is reached once the entire glacier experiences a significant speedup followed by typically strong crevassing that radically transforms the glacier surface. While the active surge (stage 3) usually lasts for few years only, stage 1 and 2 can span over a decade. Interestingly, partial surges were observed ceasing after stage 2. Despite a significant mass displacement, evidence for the event is almost exclusively given by surface elevation change. Similar phenomena that lack a sudden speedup were found on Bjuvbreen, Svalbard, (Hamilton, 1992), described as being in the quiescent phase and Trapridge glacier, Yukon, (Frappé and Clarke, 2007), termed 'slow surge'.

Further, the binary classification into surge- and non-surge type glaciers is challenged by Herreid and Truffer (2016) for Alaskan glaciers, arguing that a continuous spectrum of flow instabilities can be observed.

The application of the three-stage classification to tidewater glaciers is also challenging as earlier studies found surge initiation on tidewater glaciers to take place at the terminus without a preceding bulge formation (e.g., Murray et al., 2003). Sund et al. (2009) argued that surface elevation change of stage 1 and 2 can also be subtle, lacking a pronounced bulge and could therefore be easily overlooked. However, Sevestre et al. (2018) presented the sudden frontal initiation of two surges in Svalbard without a previous surface lowering of the reservoir area.

2.3. Surges in Heer Land

Some of the numerous past surges in Heer Land are discussed in the literature. Most prominent is the surge of Bakaninbreen in the Paulabreen system which started in 1985 (glaciers are indicated in Fig. 1.1). This surge was thoroughly studied and served as a key example for development of the theory of surges on polythermal glaciers (e.g., Murray et al., 1998). Further, the south-western tributary of Paulabreen, Skobreen surged in 2003 (e.g., Lovell and Fleming, 2023; Sund, 2006). Also, the previously mentioned slow surging Bjuvbreen is located in the area of Heer Land (Hamilton, 1992). Most recently, Moršnevbreen surged in 2016 with the evolution studied by Benn et al. (2019b). This surge is also discussed and utilized for bed inference here.

3. Methods and data

3.1. Data

Both objectives of this project, the characterization of surge dynamics and the bed inference modeling, require geospatial data from a variety of sources. The utilized data products are presented in the following.

For every bed inference run, the following data were required: Digital elevation models (DEMs) at the beginning and the end of the chosen period, a mean velocity map over the entire period, a surface mass balance map (in terms of elevation change) and a flowline along which the raster data were evaluated. The period was selected for optimal conditions of the glacier flow and data availability. Before analysis and use in the inversion, all geospatial data were transformed to a UTM coordinate system (EPSG:32633).

3.1.1. Surface elevation data

The majority of the digital elevation models used here were provided by ArcticDEM. The ArcticDEM data set (Porter et al., 2022) contains 2 m-resolution elevation data derived by photogrammetry from high resolution satellite imagery. For analysis of glacial dynamics and for visualization, DEMs were merged by the annual median in order to create overview DEMs. For the purpose of bed inference, individual stripes, captured between 2015 and 2022, were used. Generally, there were usually a few stripes available covering most glaciers every year. This made a combination of DEMs to a mosaic unnecessary and allowed for the use of individual stripes.

As the raw DEMs suffered from problems in their georeferencing, the DEMs were aligned in a preprocessing step. Here, Nuth and Kääb co-registration (horizontal and vertical translation) (Nuth & Kääb, 2011) and iterative closest point co-registration (Besl & McKay, 1992) (translation and rotation) were used. The approach was implemented by Mannerfelt (2023a).

Uncertainties in the DEMs were assessed by subtraction of two elevation models and an evaluation over stable terrain like mountain slopes, plateaus and costal flats. While the errors over flat terrain were negligible with deviations of tens of centimeters, in steep slopes differences of a couple of meters could be observed. This behavior could be attributed to the high sensitivity towards small misalignments in the co-registration in steep terrain. As the considered glaciers are flat compared to the surrounding mountain slopes, the errors in these slopes can serve as an upper limit for the uncertainty of the surface elevation change over ice. Compared to the drastic elevation changes during the surges used for bed inference of usually tens of meters per year, the uncertainties of the computed elevation changes could reach a maximum of 10 %.

Additionally to ArcticDEM, for this study we collected elevation data from Vallåkrabreen and Scheelebreen in August 2023 with an airborne laser scanner (ALS). For details, see Appendix A.

3.1.2. Surface velocity data

Surface velocity data presents a valuable tool to verify and complement surface elevation change data in order to describe glacial dynamics. For the use of bed inference, accurate mean velocity data were needed for the selected period. Because of the highly dynamic nature of a surge, temporally dense velocity measurements were required in oder to retrieve meaningful averages.

For almost all cases of bed inference, the surface velocity data from the NASA MEaSUREs ITS_LIVE project (Gardner et al., 2022) were used. The data were produced from optical satellite image pairs using the auto-RIFT feature tracking algorithm (Gardner et al., 2018), have a resolution of 240 m and cover times until 2022. For the computation of mean velocity maps, all image pair velocities with an intersection with the glacier of interest and a mid date (middle between first and second image acquisition) within the investigated period were gathered and averaged. The second image was usually captured within a few month or a whole year after the first one. The ITS_LIVE dataset contains errors for every image pair velocity estimate. These errors lay typically in the order of a few tens of meters per year (about 10 % of the velocity). However, biases introduced by data gaps were found and are discussed in Section 4.1.

Additionally, surface velocity products inferred from synthetic aperture radar were used to extend the ITS_LIVE time series. These data were provided by Adrian Luckman and are based on feature tracking on ESA Sentinel-1 image pairs from 2022 and 2023 (see Luckman et al., 2003). They are available as annual mean velocity maps for 2022 and 2023 respectively with a resolution of 100 m. For the use in bed inference, the annual means of all years during the chosen period were averaged. Years that lay only partially within a period were taken into account, weighted with the respective fraction. This procedure is much less precise than the exact selection of ITS_LIVE data per period and therefore care must be taken during the interpretation of the results. Further, this product also suffers from data gaps in the final mean. It found application only in case of the bed inference at Scheelebreen.

3.1.3. Surface mass balance data

In order to characterize the surface mass balance, the results from a glacial mass balance simulation (CryoGrid) for Svalbard, forced by meteorological reanalysis data (CARRA) were used (Dataset: Schmidt, 2022). An assessment of the elevation changes due to surface mass balance showed that during a surge the dynamic mass redistribution outweighs any mass balance by about one order of magnitude. Therefore, the influence of surface mass balance on the bed inference model is limited and the following routine aims at providing an estimate only.

For all model runs, a surface mass balance averaged over the years 2018 to 2021 was used. The simulation results are given in mass units whereas the applied bed inference model works with volume conservation. Hence, a simple conversion with a constant density factor of 850 kg/m^3 (Huss, 2013) was applied. The resulting thickening or thinning rates were interpolated from the model 2.5 km grid to a finer 50 m grid for sampling along a flowline.

3.1.4. Flowline data

As the applied Bayesian inference model is one dimensional and only informed about ice flow in the previously defined direction, the selection of a flowline is a crucial step towards the retrieval of a meaningful bed topography.

The Randolph Glacier Inventory (RGI 7.0 Consortium, 2023) features centerline data since version 7.0 which would be interesting to utilize, especially when stepping towards automatization. The new centerline data were calculated from outline and elevation data with a flow routing algorithm, presented by Kienholz et al. (2014). For some glaciers the RGI centerlines provide a reasonable estimate of a flowline. That is especially the case for the simple geometry of valley glaciers. For other glaciers, these centerlines are unsuitable for the purpose of one-dimensional bed inference due to the following limitations (see Fig. 3.1 for examples). First, the RGI centerlines of tributaries merge with the main centerline, often perpendicular, as soon as they are confluent. This contradicts the definition of a flowline as flowlines can never cross or merge. Therefore, only the main centerline can be used without manual intervention. Second, for many tidewater glaciers the terminus definition introduces an unrealistic bend in the centerline, e.g., see terminus of Kvalbreen (Fig. 3.1b). Third, a surge can massively disturb the previous flow patterns, especially if not all tributaries are surging. That might require the use of a previous tributary glacier as main centerline.

For these reasons, flowlines were newly drawn for all glaciers based on high resolution DEMs. Here, the RGI centerlines were used as a starting point, which were then corrected with signs of flow and flow direction in the form of transverse crevasses or deformed medial moraines. During the fast flow of a surge such signs are usually abundant (see Fig. 3.1).

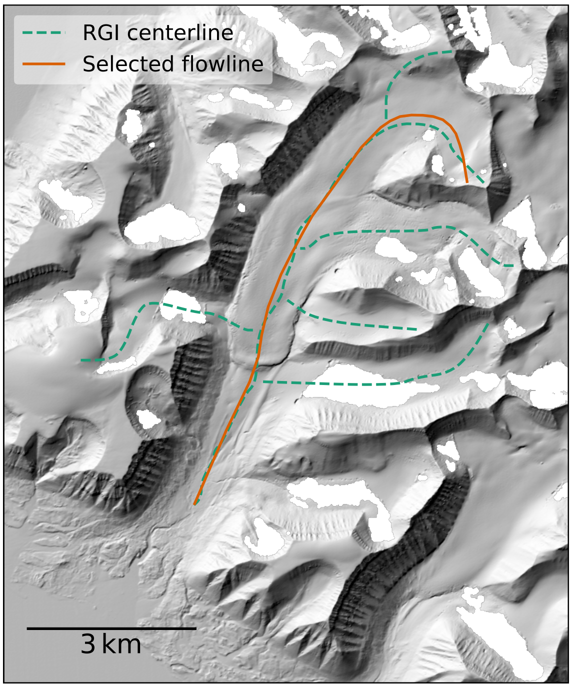

(a) Vallåkrabreen

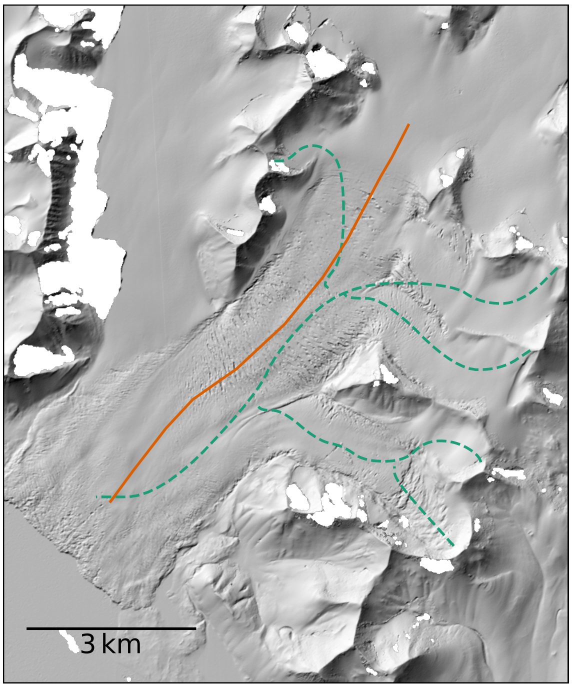

(b) Kvalbreen

Figure 3.1.: Centerlines from the Randolph Glacier Inventory (RGI) and flowlines used for bed inference. The usability of RGI centerlines as flowlines varies strongly. Here, only on Vallåkrabreen an application as flowline would be possible. The background shows ArcticDEM stripes from April 2022.

3.1.5. Satellite imagery

Optical satellite images are a valuable tool to qualitatively characterize glacier motion, terminus position and crevassing. Modified Copernicus Sentinel-2 data (2016–2024) processed by Sentinel Hub were used to help in the reconstruction of surge sequences.

3.2. Bed inference modeling

3.2.1. Overview

The inverse modeling approach applied here was introduced by Brinkerhoff et al. (2016). Morin et al. (2023) further developed the model and showed how the high-slip flow during a surge poses favorable conditions for bed retrieval.

For this approach a single flowline (the theoretical path of an ice parcel in the glacial flow) was chosen along which all evaluations were performed. The set of model parameters contains ice thicknesses, surface elevation changes, surface velocities and other variables at locations along the flowline which are all related via the continuity equation. During the Bayesian inversion the model parameters were determined that are most likely given the available observations. In this process a random set of model parameters was generated (excluding surface velocity) and used to compute the surface velocities using the continuity equation. In a following step these model parameters were compared against observations of the same parameters (where available) and prior knowledge about their spatial variability. Using the Metropolis-Hastings algorithm, many of such sets of random model parameters were generated and evaluated leading to a probability distribution for every parameter at every location along the flow line. From these distributions mean and standard deviation of the parameters could be computed in order to retrieve ice thickness estimates.

3.2.2. Continuity model

The forward model used for inversion simply follows mass conservation along a single flowline, i.e., it evaluates the one-dimensional continuity equation.

We start with the two-dimensional continuity equation

$$\frac{\partial S(\boldsymbol{x})}{\partial t} = -\nabla \cdot \left(\bar{U}(\boldsymbol{x})H(\boldsymbol{x})\boldsymbol{N}(\boldsymbol{x})\right) + \dot{b}(\boldsymbol{x}), \tag{3.1}$$

where $S(\boldsymbol{x})$ is the surface elevation at a location $\boldsymbol{x} = (x, y)$, $\bar{U}$ the depth averaged velocity, H the ice thickness, $\boldsymbol{N}$ the flow direction vector and $\dot{b}$ the surface elevation change due to surface mass balance. At this point we assume that basal melt is negligible, that the bed elevation is constant over time (no bed erosion) and that the flow direction is constant over the entire depth.

Reducing the continuity equation to one dimension along a specific flowline gives

$$\frac{\partial}{\partial r}\left(w(r)\bar{U}(r)H(r)\right) = w(r)\left(\dot{b} - \frac{\Delta S(r)}{\Delta t}\right) \tag{3.2}$$

with the new coordinate r giving the distance from the glacier head. The lateral divergence is now taken care of by the flowline width w. This width can be seen as the distance between two neighboring flowlines and is inferred during the inversion as a free parameter. Note that in this step also an integration over time has been performed, replacing the time derivative with a difference quotient and all other quantities with their temporal average over the observation period. We now replace the depth averaged velocity $\bar{U}$ by the surface velocity $U(r) = s\,\bar{U}(r)$, introducing a constant conversion factor s, the slip factor which is determined as an additional parameter during the inversion. Integration along the flow line yields

$$\frac{U(r)}{s} w(r) H(r) = \int_0^r w(r') \left(\dot{b}(r') - \frac{\Delta S(r')}{\Delta t} \right) dr'. \tag{3.3}$$

Here, it is instructive to have a look at the individual terms in this equation. It can easily be seen that the left-hand side represents the ice flux through a cross section of the flowband at distance r. The integral on the right-hand side accounts for the accumulated surface lowering upstream of r, corrected for accumulation or ablation. Therefore, the conditions at every point on the flowline (left hand side) are related to the conditions upstream only. Consequently, it can be seen that the influx of ice at the glacier head ($r = 0$) is assumed to be zero. The boundary condition at the terminus, however, is left unconstrained and is irrelevant for the model.

A simple rearrangement of Equation 3.3 gives an expression for the surface velocity

$$U(r) = \frac{s}{w(r)H(r)} \int_0^r w(r') \left(\dot{b}(r') - \frac{\Delta S(r')}{\Delta t} \right) dr'. \tag{3.4}$$

This form of the one-dimensional continuity equation is used by the forward model for computation of surface velocities. A more thorough derivation is given by Brinkerhoff et al. (2016).

3.2.3. Bayesian inference

The goal of Bayesian inference is to characterize the posterior probability distribution $P(\boldsymbol{m}|\boldsymbol{d})$. The posterior is the probability to find a model in a state characterized by the model variables $\boldsymbol{m}$ given observations $\boldsymbol{d}$. The model variable vector $\boldsymbol{m}$ contains the entire state of the model, i.e., the set of model variables for every point along the flow line as listed in Table 3.1. The observation vector $\boldsymbol{d}$ contains measurements of the same model variables at specific locations along the flow line. Bayes' theorem

$$P(\boldsymbol{m}|\boldsymbol{d}) \propto P(\boldsymbol{d}|\boldsymbol{m})P(\boldsymbol{m}) \tag{3.5}$$

allows us to relate the posterior to the likelihood $P(\boldsymbol{d}|\boldsymbol{m})$ and the prior $P(\boldsymbol{m})$. The likelihood is the probability for the model to result is an observed state $\boldsymbol{d}$ given a configuration of model parameters. $P(\boldsymbol{m})$ is the probability distribution that contains prior knowledge about the model variables which is not contained in the observations.

Table 3.1.: List of model variables and hyper-parameters used for inversion (see Eq. 3.4). Amplitude σ_{Gp} and length scale l_{Gp} characterize the Gaussian process priors while the observation uncertainty σ_{obs} determines the influence of observations on the model. Note that the surface velocity is not modeled as a Gaussian process but computed from the other variables via the continuity equation.

	Variable	σ_{Gp}	l_{Gp}	σ_{obs}
$S(r)$	Surface elevation	200 m	500 m	5 m
$S(r) - H(r)$	Bed elevation	200 m	500 m	10 m
$\Delta S/\Delta t(r)$	Surface elevation change	50 m	500 m	5 m
$\dot{b}(r)$	Surface mass balance	10 m	500 m	5 m
$w(r)$	Flowline width	0.05 m	500 m	-
$U(r)$	Surface velocity	-	-	50 m/yr
s	Slip factor	-	-	-

Here, priors are used to input knowledge about the typical length scale and spatial variability of a variable in the form of Gaussian processes. For every two points r and r' the Gaussian covariance function

$$K(r, r') = \sigma_{Gp}^2 \exp\left(-\left(\frac{r - r'}{l_{Gp}}\right)^2\right) \tag{3.6}$$

applies. Where needed, also non-negativity constraints are used (e.g., ice thickness and velocity). The amplitude σ_{Gp} and length scale l_{Gp} are considered hyper-parameters. Additionally, the uncertainties of the observations σ_{obs} are part of the set of hyper-parameters that needs to be adjusted to fit the specific glacier and variable. These hyper-parameters can also be seen as a regularization method that forces the model to simple solutions. An overview over the selected values can be found in Table 3.1.

3.2.4. Implementation

The retrieval of the posterior is done by sampling the distribution. Here, the Metropolis-Hastings algorithm (Hastings, 1970), a Monte Carlo Markov chain method, is used to draw individual samples.

This algorithm requires a function $f(\boldsymbol{m})$ proportional to the desired distribution (the posterior). Exploiting Bayes' theorem (Eq. 3.5), we can write f as the product of likelihood and prior:

$$f(\boldsymbol{m}) = P(\boldsymbol{d}|\boldsymbol{m})P(\boldsymbol{m}) \propto P(\boldsymbol{m}|\boldsymbol{d}). \tag{3.7}$$

This expression is lacking a closed form but can be evaluated pointwise. During the evaluation for a given state $\boldsymbol{m}$, the continuity equation (Eq. 3.4) is used to compute the corresponding surface velocity. A comparison with the observations and computation of the Gaussian covariance function (Eq. 3.6) results in estimates for the likelihood and the prior distribution and therefore for f.

The algorithm is initialized by selecting an arbitrary starting point $\boldsymbol{m}$ of model variables. During the sampling, the algorithm is traveling through the model parameter space, similar to the random walk. In every step, the next candidate $\boldsymbol{m'}$ is proposed in the vicinity of the current sample $\boldsymbol{m}$ according to a proposal function $q(\boldsymbol{m'}, \boldsymbol{m})$. Here, a multivariate normal distribution is used. The proposed sample is accepted if $f(\boldsymbol{m'}) > f(\boldsymbol{m})$, i.e., when the posterior increases. If the posterior decreases ($f(\boldsymbol{m'}) \leq f(\boldsymbol{m})$), the candidate is accepted only with a probability of $f(\boldsymbol{m'})/f(\boldsymbol{m})$. After running the algorithm, a collection of samples (model states) is gained. The probability distribution of each parameter can be visualized by a histogram, the mean value and standard deviation are computed for further evaluation. Here, three runs of 10^6 iterations are used of which the first 10^5 samples are discarded as a spin-up. Further, only every tenth sample is kept in order to prevent correlation between samples. The convergence of the algorithm can be assessed by comparing the variance of each of the three chains to the total variance (Gelman-Rubin statistics).

Here the model implementation from Morin et al. (2023) is used which is based on the python library `PyMC` (Abril-Pla et al., 2023).

3.3. Ground penetrating radar

Ground penetrating radar (GPR) data can be used to gain information about the true ice thickness and to verify results from bed inference modeling. From the glaciers studied here, only Vallåkrabreen was surveyed in recent years. On Vallåkrabreen GPR was done in May 2021 by Andrew Hodson (University Center in Svalbard) with a 100 MHz antenna. These unpublished data were used for the first time.

The preprocessing of the GPR data was done with `rsgpr` (Github: Mannerfelt, 2023b) and involved a conversion of the data to equal-distant steps. The vertical axis was converted from time domain to depth using a wave velocity in ice of 168 m/µs (Petrenko and Whitworth, 1999). From the depth coordinates the elevation above sea level was computed by using surface elevations from the ArcticDEM median from 2021. For visualization the centerline survey, which was recorded in two sections, was stitched together. The result is shown in Figure 3.2.

The majority of the glacier bed shows a clear reflection that can be used to determine ice thickness. Only in the upper-most region are multiple bed reflections visible, most likely caused by reflections from the side of the glacier due to the bed geometry. In cases with multiple reflections the strongest one is chosen as the true bed. The deviation between multiple reflections never exceeds 10 % of the ice thickness and is therefore negligible for purposes of this study.

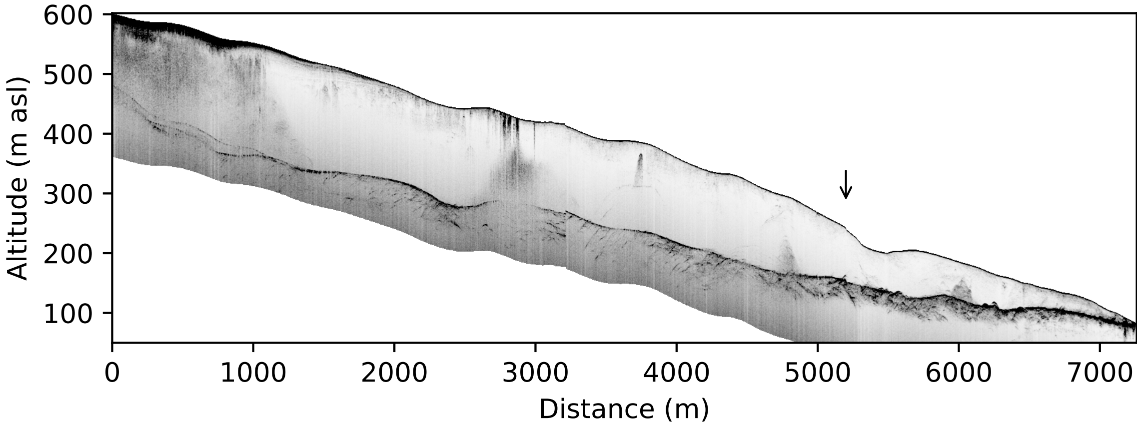

Figure 3.2.: Radar profile of Vallåkrabreen along centerline with a mostly clear reflection from the glacier bed (dark). Ambiguous reflections are present in the uppermost 1000 m only. The ground penetrating radar data (100 MHz) were collected in May 2021 during the early surge by Andrew Hodson. The down glacier propagating surge bulge is indicated by an arrow.

In order to display the known bed topography along arbitrary cross sections (e.g., a flowline), the bed elevation was interpolated between all survey lines. However, only places no further than 100 m from a radar measurement were used as reference. The corresponding ice thicknesses are shown in Figure 3.3.

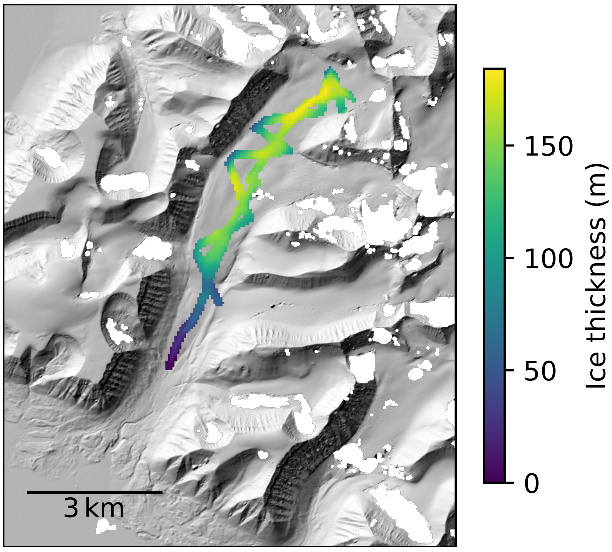

Figure 3.3.: Interpolated ice thickness of Vallåkrabreen from radar survey in 2021. The data were interpolated to all locations no further than 100 m from the measurements. The background DEM (ArcticDEM) was captured in April 2021.

4. Results

4.1. Biases in velocity data

Before presentation of results from first and second objective, a thorough discussion of the used velocity data is required, due to the existence of potentially severe biasses.

As Morin et al. (2023) already mentioned, ITS_LIVE data become unreliable during a surge. Further, during the processing of velocity data, artifacts like sharp borders or unrealistically low velocities were noticed. Therefore, and for the need of accurate velocity means, the potential of the ITS_LIVE dataset for bed inference is evaluated here.

During the fast flow regime of a surge, a correlation between no-data pixels and glacier speed can be observed in some cases. An example is shown in Figure 4.1, where ITS_LIVE image pair velocities are averaged to monthly means during the surge of Scheelebreen. In August 2021, the surge reached the previous terminus causing Scheelebreen to advance rapidly in the following months. During this period, no single image pair covered the fast flowing glacier tongue, causing severe biases in any long-term mean velocity covering this period. Interestingly, the correlation between data gaps and fast flow is so strong that the terminus advance is visible as an expansion of data gaps.

As ITS_LIVE is based on the comparison of optical image pairs, the gaps are most likely caused by the lack of imagery during the polar night. The fast change of surface texture during a surge (e.g., sudden terminus advance or crevassing) could make correlation of image pairs impossible for periods greater than a few months or even less. In

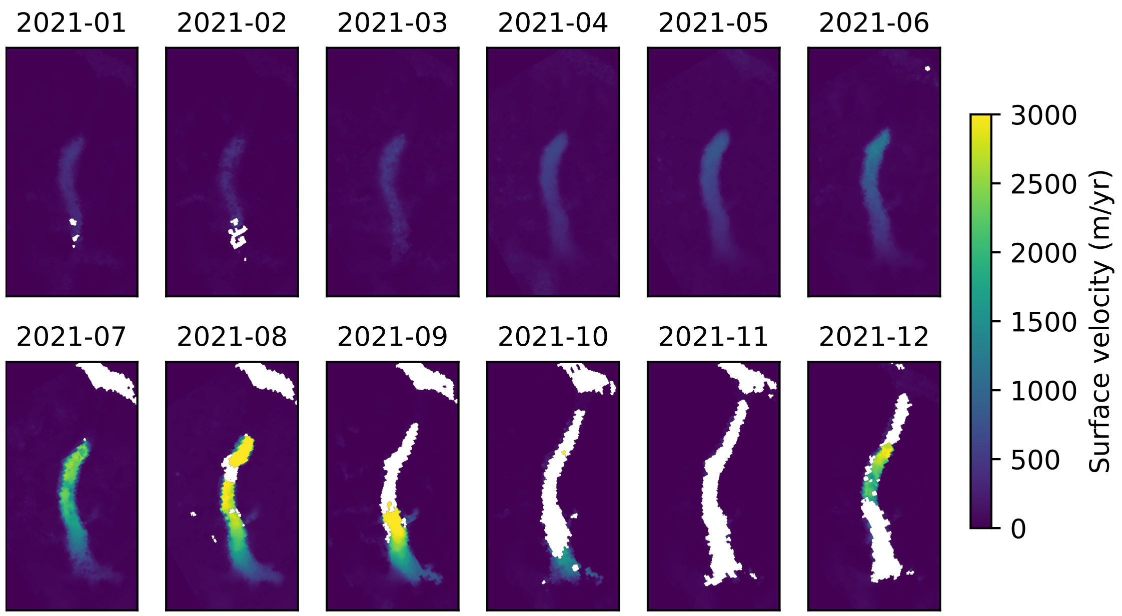

Figure 4.1.: Monthly mean velocities of Scheelebreen from ITS_LIVE. No-data gaps are consistently present over fast moving regions like the advancing terminus. These gaps can lead to significantly biased mean values for longer periods.

general the polar night is not causing issues or data gaps as long as images as before and after can be matched.

A way to mitigate biases is to use periods with good data coverage only. In Figure 4.2, the glacier wide velocity mean is plotted as a time series together with the amount of no-data pixels within the glacier outline. Each quantity was calculated for short term averages (10 days), for the spatial means the glacier outlines from the Randolph Glacier Inventory (RGI 7.0 Consortium, 2023) were used. This visualization of short-term averages presents a convenient way to discover and to quantify potential bias problems. Here, it allows for a convenient selection of a suitable time window for further use.

From Figure 4.2 it can be observed that mainly Moršnevbreen (but also Arnesenbreen and Kvalbreen) features an extended period of very high velocities and almost no missing data towards the end of the surge. Such periods have a great potential for the use in bed inference. A reason for the better performance of the ITS_LIVE feature tracking algorithm could be that towards the end of a surge, high velocities and crevasses are

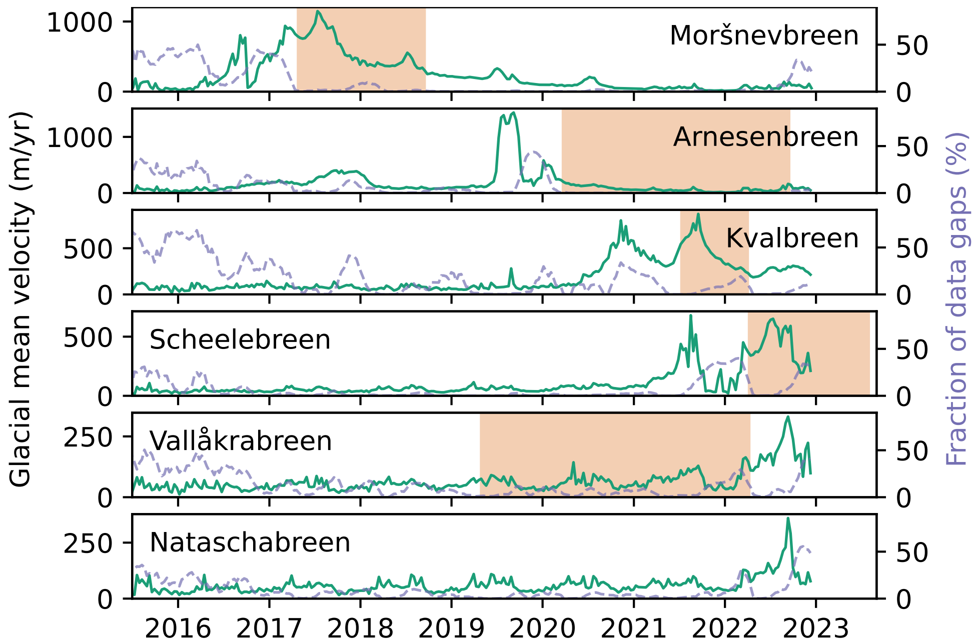

Figure 4.2.: Time series of ITS_LIVE velocities (green) and the corresponding size of spatial data gaps (gray). All glaciers feature sudden velocity increases caused by a surge. The number of no-data pixels can be a good indication for potential biases in the averaged velocity data. Periods selected for bed inference are shaded. The time series was calculated for each glacier from image pair velocities which were averaged over the entire glacier area (RGI outline) and a ten-day period. The fraction of data gaps was averaged over 50 days.

established glacier-wide. Further, also the size of the glacier might play a role in how well trackable features are preserved during a surge, as for large and wide glaciers less disturbance from the margins is to be expected. Both results in a more uniform, feature-rich flow, where crevasses can even be tracked by eye on DEMs over the course of multiple years.

4.2. Glacier dynamics

The diverse glacier dynamics in the region of Heer Land can be studied from the good spatial and temporal cover of ArcticDEM stripes. Resulting surface elevation changes, based on a subtraction of annual medians from the years 2018 and 2021 are shown in Figure 4.3. On this map a variety of glacial dynamics becomes observable.

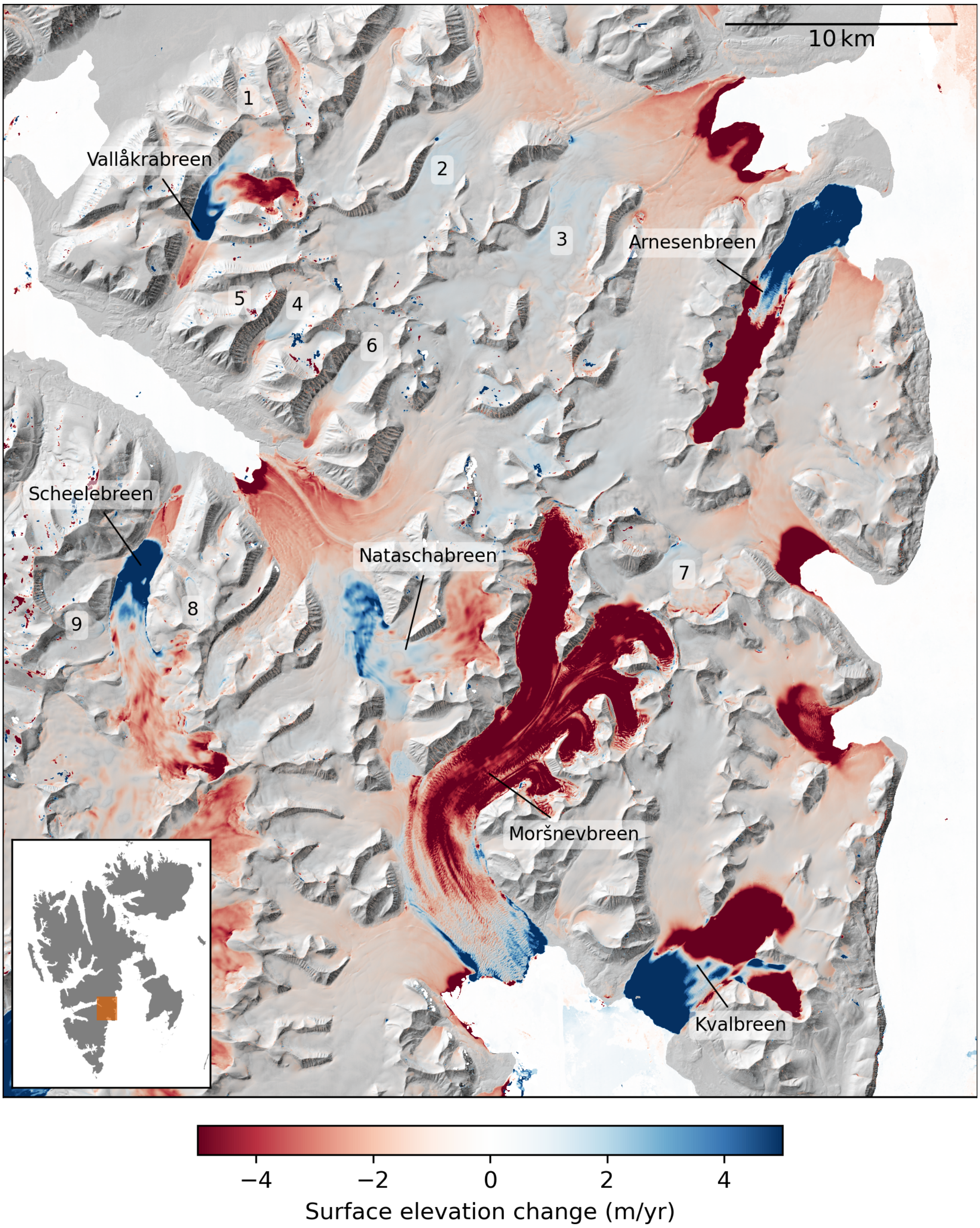

Figure 4.3.: Surface elevation change between 2018 and 2021 in Heer Land. For the six active surges (labeled), the mass redistribution towards the receiving area is clearly visible. Note that some areas of heavy elevation change (up to 30 m/yr) are far beyond the limits of the color bar. Additionally, glaciers with surge-like dynamics are numbered (see Tab. 4.1). Elevation change is calculated by subtraction of ArcticDEM annual medians. The median DEM from 2021 is shown in the background.

Table 4.1.: Glaciers in Heer Land with surge-like behavior between 2016 and 2024, sorted north to south. The timing of stage 3 is roughly estimated because the onset can be gradual. The area is adopted from the RGI or estimated for the tributaries.

Glacier	Location	Area (km^2)	Speedup (stage 3)	Comment
Bjuvbreen (1)	77.9063°N, 17.2141°E	1	-	bulge, advancing
Edwardbreen (2)	77.8775°N, 17.5625°E	61	-	
Vallåkrabreen	77.8740°N, 17.1516°E	22	2023	bulge preceding surge
Nordsysselbreen (3)	77.8589°N, 17.7976°E	64	not yet	advancing in 2024
Mettebreen (4)	77.8309°N, 17.2808°E	8	-	bulge
Lognbreen (5)	77.8300°N, 17.1631°E	2	-	bulge, advancing
Arnesenbreen	77.8211°N, 18.1363°E	24	2016	terminus initiated surge
Ragna-Mariebreen (6)	77.8042°N, 17.3902°E	10	-	bulge
Vigilbreen (s. tributary, 7)	77.7192°N, 17.9641°E	~ 7	-	
Klubbebreen (8)	77.7128°N, 17.0765°E	2	-	bulge
Scheelebreen	77.7111°N, 16.9595°E	47	2021	bulge preceding surge
Nataschabreen	77.7047°N, 17.3588°E	60	2024	bulge preceding surge
Fredbreen (n. tributary, 9)	77.7017°N, 16.8629°E	~ 2	-	bulge, advancing
Moršnevbreen	77.6651°N, 17.6719°E	120	2016	bulge preceding surge
Kvalbreen	77.5782°N, 18.0325°E	33	2020	terminus initiated surge

4.2.1. Currently not-surging glaciers

This section aims at describing all glaciers that are not in a fully developed surge state like quiescent glaciers but also glaciers with a dynamic behavior that does not directly qualify as a surge.

Heer Land features wide regions with slightly positive surface elevation change in the accumulation area. This can be observed especially for glaciers that surged during the last decades (e.g., Skobreen and Bakaninbreen, north-eastern and south-western tributary of Paulabreen respectively) and can be seen as a recovery from the surge during the quiescence.

Further, a great number of glaciers with surge-like behavior can be detected, mostly from the elevation change between 2018 and 2021. A list of those is given in Table 4.1. Here, the term surge-like shall include all glacial mass redistribution that is characterized by a local thickening accompanied by surface lowering higher up on the same glacier. This can include surge stage 1 and 2 (by Sund et al. (2009)) with more or less pronounced bulges. Most glaciers with an accumulation area south-east of Vallåkrabreen show such a behavior. The relatively small glaciers Mettebreen and Ragna-Mariebreen flowing to the south-west already developed bulges. Edwardbreen and Nordsysselbreen (flowing north-east) are much bigger and show gentle but wide spread thickening in the middle, while individual upper cirques are lowering. On Sentinel-2 imagery from 2023 and 2024, acceleration, deformation of medial moraines and the appearance of shear margins are observable at Nordsysselbreen, indicating the potential start of a (stage 3) surge.

Also very small glaciers in the region show surge-like behavior. This group of glaciers, no bigger than 1–2 km^2, shows local thickening due to a propagating bulge. Bjuvbreen, Lognbreen, Klubbebreen and Fredbreen (north to south) fall into this category and are indicated in Figure 4.3. In many cases the bulge already reached the former terminus, causing the glacier to start advancing. It is also worth mentioning that Bjuvbreen is thought to have surged before and was thoroughly studied during the buildup of the current bulge (Hamilton, 1992). Even more, mostly nameless glaciers, with similar behavior, though less pronounced, can be found upon closer inspection but are not included in Table 4.1.

4.2.2. Active surges

In Figure 4.3 a total of six full-grown surges (labeled) are visible due to the enormous mass transport from the reservoir to the receiving area. Following Sund et al. (2009), these glaciers can be classified as stage 3 surges. The timing of these surges can best be read from Figure 4.2.

Moršnevbreen is a main tributary of the Strongbreen system and tidewater terminating. The chronology of this surge is well documented by Benn et al., 2019b During its surge, years before the main speedup, a down-glacier propagating bulge could be observed. The entire glacier started a sudden speed up when the bulge reached the vicinity of the terminus in summer 2016. After velocities peaked, a three-year-long phase of gentle deceleration started.

At Arnesenbreen, on the other hand, no evidence of any bulge could be found. This surge started in 2016 with enhanced velocities and surface lowering at the terminus,

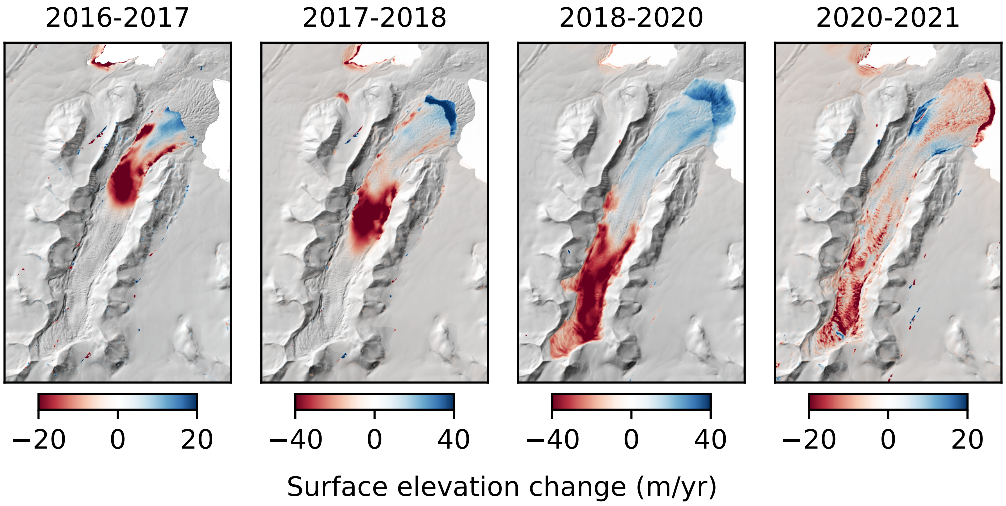

Figure 4.4.: Arnesenbreen: Surface elevation change during the surge. The acceleration took place in two steps in 2017 (lower half) and 2019 (entire glacier). Towards the end of the surge (2020–2021) ice was diverted to the sides of the terminus instead of contributing to further advance. Background: ArcticDEM 2021.

propagating up-glacier (see Fig. 4.4). Interesting in this case is that the upwards propagation only reached the middle of the glacier, leaving the upper glacier untouched for roughly a year. After a period of surge velocity reduction, Arnesenbreen saw another speedup in summer 2019, this time affecting the whole glacier. However, compared to Moršnevbreen, this surge ceased quickly within a year. Towards termination, Arnesenbreen showed a glacier-wide block of ice at the terminus that stopped moving while the main glacier continued delivering ice. This forced the ice flow to be directed towards the sides of the glacier and is visible as positive elevation change limited at the lateral margins in Figure 4.4.

Kvalbreen, similarly to Arnesenbreen, appeared to initiate a surge from its terminus with no bulging observable in the years before the surge. The evolution of this surge can be studied from the time series of elevation change and surface velocity, shown in Figure 4.5. After velocities started to increase at the tidewater margin, the surge propagated upwards speeding up the whole glacier in summer 2020.

Scheelebreen and Vallåkrabreen are the only land-terminating glaciers included in this study. Both featured a well pronounced bulge during the early stages of the surge, both

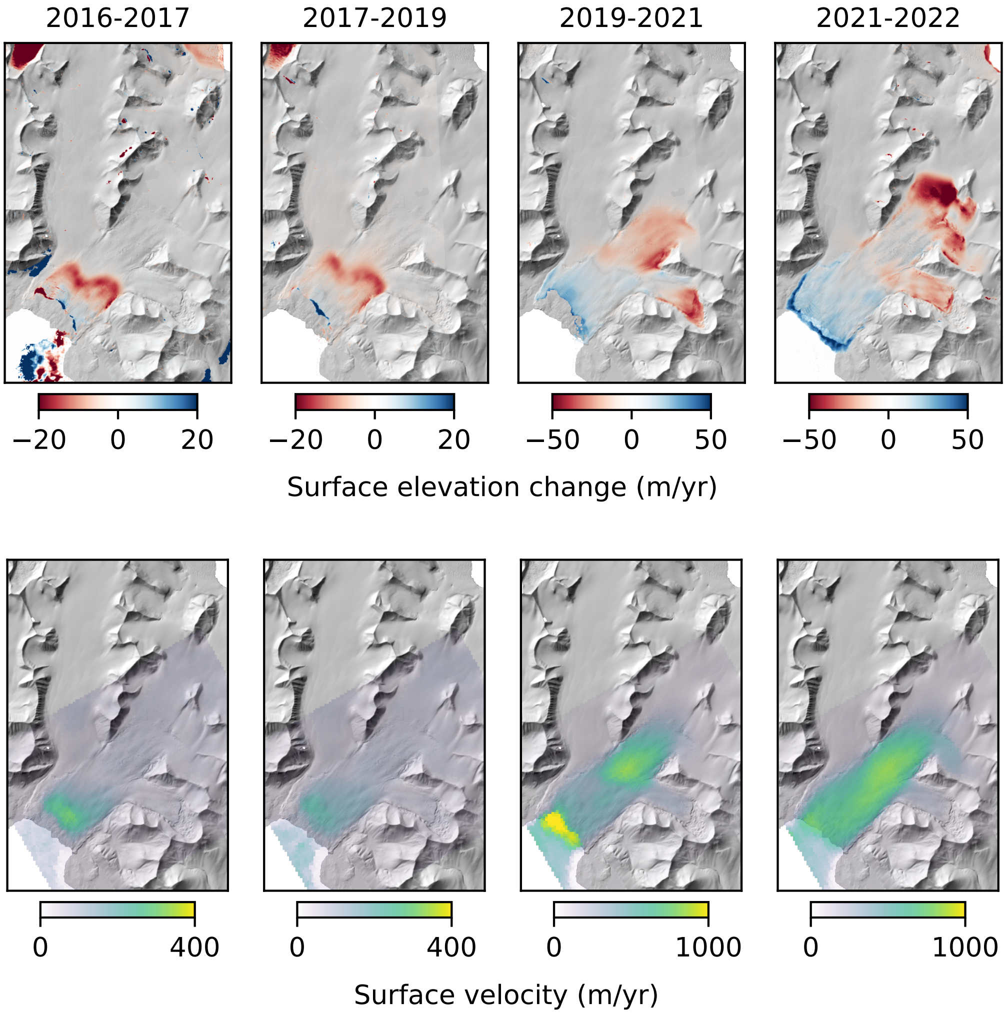

Figure 4.5.: Kvalbreen: Surface elevation change and surface velocity during the surge. The upstream propagation of a surge front can be observed before a glacier-wide acceleration took place in 2020. Background: ArcticDEM 2021.

visible in Figure 4.3. The formation of the bulges started slow and took many years. Even if the ice upstream of the surge front gradually accelerated, the sudden speedup did not happen before the bulge reached the terminus. This happened in August 2021 (see Fig. 4.1) for Scheelebreen and in early 2023 for Vallåkrabreen. For Vallåkrabreen, the last years of the buildup of the bulge are presented in the time series of elevation change and surface velocity in Figure 4.6. Due to its advance, Scheelebreen turned into a tidewater glacier only 6 months after it reached the former terminus.

Nataschabreen, a tributary of the Paulabreen system, developed a surge bulge since at

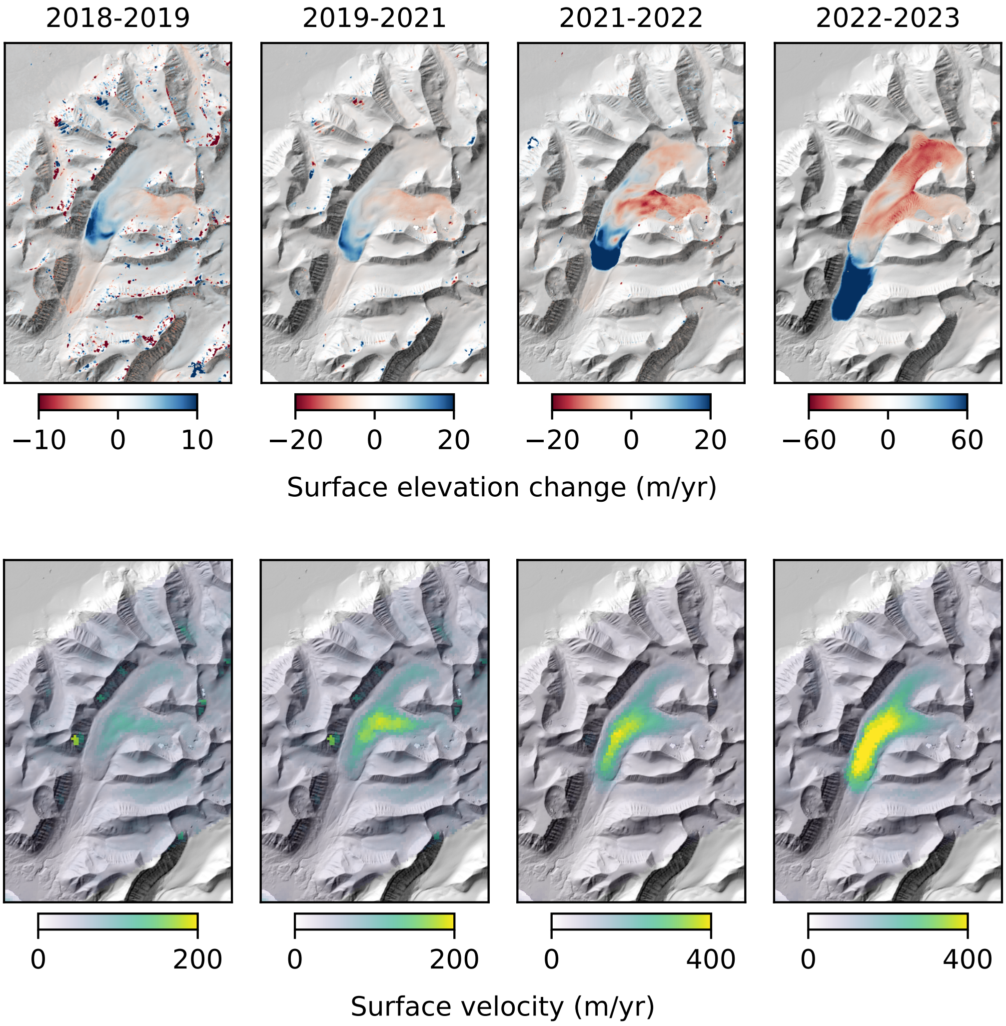

Figure 4.6.: Vallåkrabreen: Surface elevation change and surface velocity during the surge. The development of a surge bulge in the Firmbreen tributary can be observed. Background: ArcticDEM 2021. Note that the ITS_LIVE velocity time series ends after 2022, therefore the last velocity map covers only half the given period.

least 2018 and showed slowly rising velocities in 2022. In summer 2024, satellite pictures showed the surge front to have reached the terminus causing a glacier-wide acceleration and advance. As this surge is at the time of this study just in the process of developing, it was not used for the purpose of bed inference.

4.3. Bed inference

In Bayesian inference, the model output is given as samples of the model parameters representing the posterior distribution. In order to evaluate the results, mean and standard deviation of each parameter at each location along the flowline are computed and plotted along the observations of the same parameters. The inversion results are shown for the example of Vallåkrabreen for all parameters in Figure 4.7. For all other glaciers the full results can be found in Appendix B. These plots provide a good overview over the model behavior as they visualize to which degree the individual parameters are constrained by observations or inferred via the continuity equation.

The sensitivity of the model towards changes in the hyper-parameters was tested for the bed elevation prior as this represents an important parameter with direct influence on the modeled bed topography. For the additional two inversion runs, the Gaussian process bed amplitude σ_{Gp} of 200 m, as it was set in all other runs, was increased and decreased by 100 m respectively. The results are shown for two of the glaciers Vallåkrabreen and Moršnevbreen in Figure 4.8. Surprisingly, the two cases show widely different responses to the change in the bed prior.

For Vallåkrabreen, the adjustment leads to a dramatic change in ice thickness, which strongly limits the trust in the retrieved values as the mean bed elevation can be chosen almost arbitrarily. However, it is also worth pointing out that the general uncertainty is very high in case of Vallåkrabreen and that the results with altered prior are still within the standard deviation. Moršnevbreen, on the other hand, does not show any significant variation in ice thickness estimates after the manipulation of hyper-parameters. This glacier also features a much lower standard deviation of the bed elevation. Therefore, the estimated standard deviation prove to be a valuable tool to asses the quality of the results, as the problem of extreme sensitivity on hyper-parameter variations is limited to cases with a high uncertainty. This suggests, that these problems are caused by a lack of information in the input data and not of the model itself.

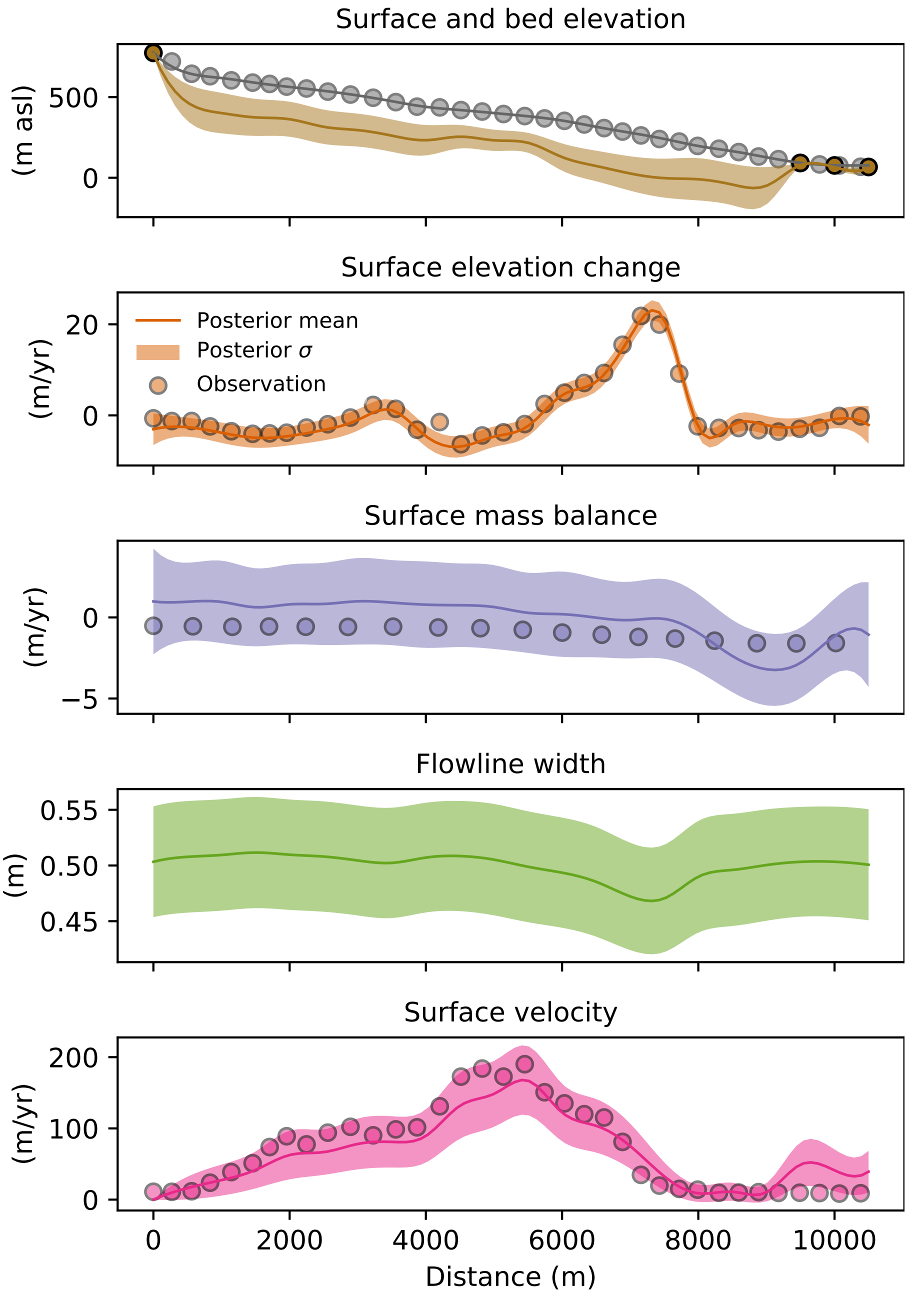

Figure 4.7.: Bayesian model input (observations) and output (mean and the standard deviation) for Vallåkrabreen given for each model parameters. Upper panel: The results of surface elevation (gray) and bed elevation (brown) can be seen as cross section along the flowline. While the surface is entirely constrained by observations, bed observations are only available at the boundaries of the glacier. Hence, the estimated bed is fully based on the other parameters. Lower panels: Observations and results of the other model parameters. As visible, also the modeled width of the flowline is not constrained by data.

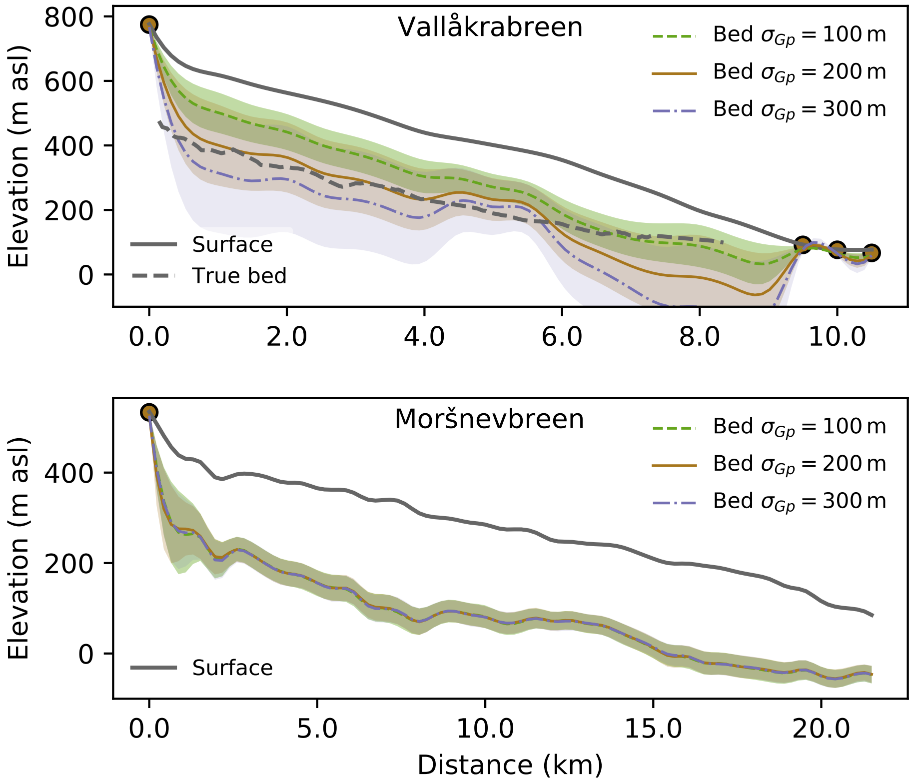

Figure 4.8.: Influence of hyper-parameter variations on inversion results. The posterior mean is shown for three inversions with differently set priors for the bed amplitude σ_{Gp}. The shadings indicate the standard deviation of the posterior and the dots the limits of the glacier where the bed is constrained.

As the surging glaciers that are used for bed inference show very different geometries, surge evolution and data coverage, the results are individually discussed here. All resulting bed topographies, shown in Figure 4.9 - 4.11 use the same scale for comparability.

4.3.1. Vallåkrabreen

The surge of Vallåkrabreen is the most recent one covered here. As both the ArcticDEM and the ITS_LIVE velocity time series end after 2022, the available data, especially for late surge phases, is very limited. Therefore, an early period before the major speedup was chosen which includes the down-glacier advance of the surge bulge. Vallåkrabreen is an especially interesting candidate as the ice thickness is known for large parts of the glacier due to a radar survey in 2021 (see Sec. 3.3). Further, it is a typical land terminating valley glacier with well defined head and terminus. For these reasons, Vallåkrabreen could serve as a test for model performance.

The bed topography resulting from the inversion (Fig. 4.9) shows a very high standard deviation and highly unrealistic bed elevations in the lower half of the glacier. Most likely, this behavior can be attributed to the following problems. First, as the used time span includes the bulge propagation, it can be assumed that very different flow regimes are present within the glacier. E.g., the terminus is unaffected by the surge and therefore frozen to the bed while the ice upstream the bulge is seeing an acceleration. Second, velocity biases play an important role, also in this period Underestimated velocities usually lead to overestimated ice thicknesses. Third, the surge was initiated in

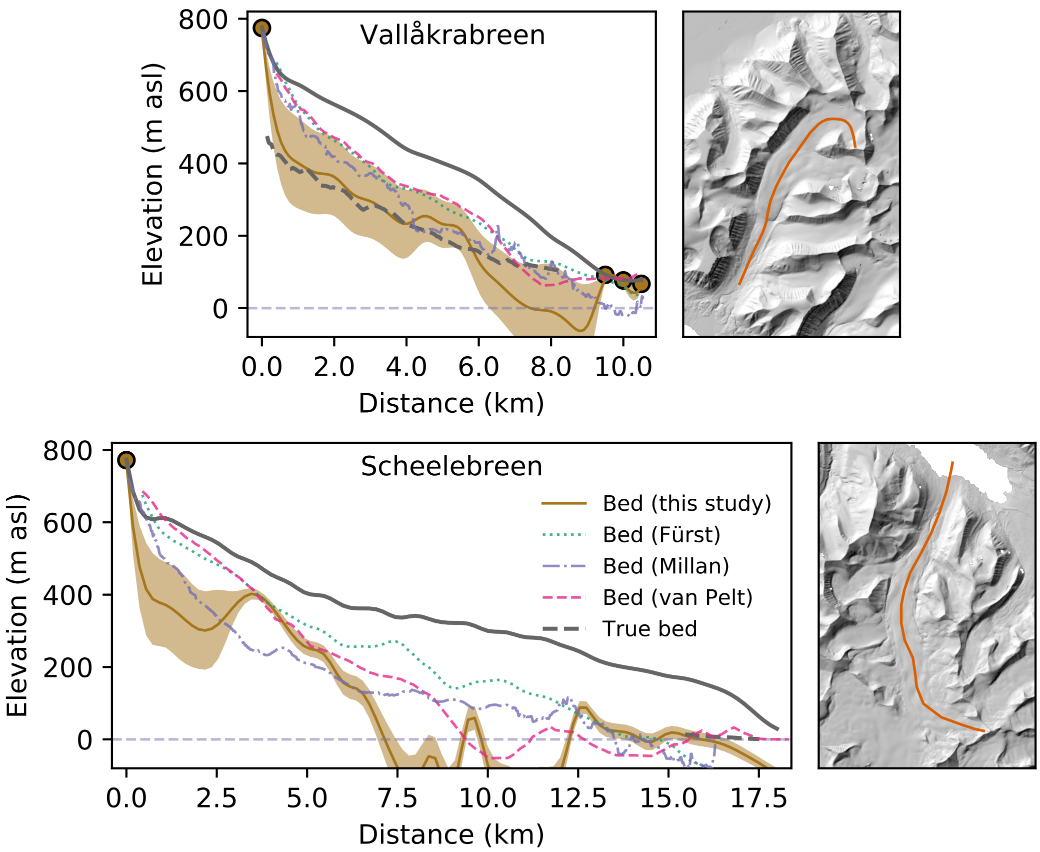

Figure 4.9.: Resulting surface (gray) and bed elevation (brown, with uncertainty) along one flowline (right panel) and comparison with the bed topography from Fürst et al. (2018), Millan et al. (2022) and van Pelt and Frank (2024). Figure 4.9 - 4.11 use the same scale for comparability, the depiction of elevation is exaggerated by a factor of ten.

Firmbreen, an eastern tributary creating an enhanced ice flux into the main stream, further complicating the ice flow. This can explain the problems in the lower glacier (after a distance of 4000 m) as velocity and elevation change in this area are governed by the ice originating from Firmbreen, an area the model is not informed about. A comparison with the true bed shows that low deviations can be reached for the upper-most part with the right set of hyper-parameters. However, the systematic problems and the sensitivity towards changes in hyper-parameters (demonstrated above) would make a quantitative comparison between model results and true bed meaningless.

4.3.2. Scheelebreen

To avoid the problems during the early surge stage found at Vallåkrabreen, I chose a later period for Scheelebreen that requires additional data, extending the ArcticDEM and the ITS_LIVE velocity time series. Therefore, the synthetic aperture radar derived velocities and the acquired laser scanner DEM were used. Also for Scheelebreen, a small section of the bed is known that can be used for the assessment of the results. The known bed results form the non glacierized land surface predating the surge.

The modeled bed topography (Fig. 4.9) is dominated by unrealistically strong fluctuations of the bed elevation. Most of the sudden jumps can be traced back to problems in the velocity data like gaps or jumps. However, the standard deviation is comparatively low which could show that the fast flow of Scheelebreen is generally suited for bed inference applications. Further, the comparison to the true bed close to the terminus shows high agreement at about 16 km, suggesting that the much higher velocity in the area is correct. The deviation, increasing down-stream is caused by the widening of the glacier towards the sea, which is not adequately modeled.

The inversion was executed with the glacier bed only confined at the glacier head as the terminus is calving into the sea during the period. Even if the known bed could have been used as a bed observation, the model manages well to reproduce the bed at this location without this constraint. This means that the unquantified outflow of ice in the form of calving is not limiting the model. Only this small but important fact allows the application of the model to other tidewater glaciers.

4.3.3. Kvalbreen

For the bed inference of Kvalbreen, a period was chosen where the surge affected the whole glacier and led to a glacier-wide speedup. Even if these conditions, accompanied with decent velocity data are favorable for the inversion, the glacier geometry is challenging. The glacier is not limited by a head nor is it land terminating but it drains a small ice cap and terminates in tidewater. However, the uppermost region was stagnant and did not show significant surface elevation change, enabling the application of continuity.

See Figure 4.10 for the results. As expected, the uppermost region with little ice motion shows a higher uncertainty than the rest of the glacier, where uncertainties are significantly smaller, confirming the suitability of the flow conditions for the inference. As Kvalbreen is tidewater terminating, the true bed elevation at the terminus is below sea level. The model fails in reproducing this and is therefore off by about 50 m or more.

4.3.4. Arnesenbreen

The period chosen for the bed inference lays after the main surge where velocities slowly returned to normal levels. Due to the presence of severe velocity biases, the main surge could not be exploited.

Compared to the other glaciers, the inversion results (see Fig. 4.10) show a high standard deviation. Also in this case, it is likely that the slower glacier motion, with potentially less slippage is less suited for the purpose of bed inference. Further, low bed elevations of multiple hundred meters below sea level highlight problems towards the terminus as nautical charts Kartverket (2024) suggest depths of roughly 20 m. From the velocity data and a comparison of DEMs (see Fig. 4.4), it can be seen that the last 2.5 km from the terminus stopped moving before the rest of the glacier did. This

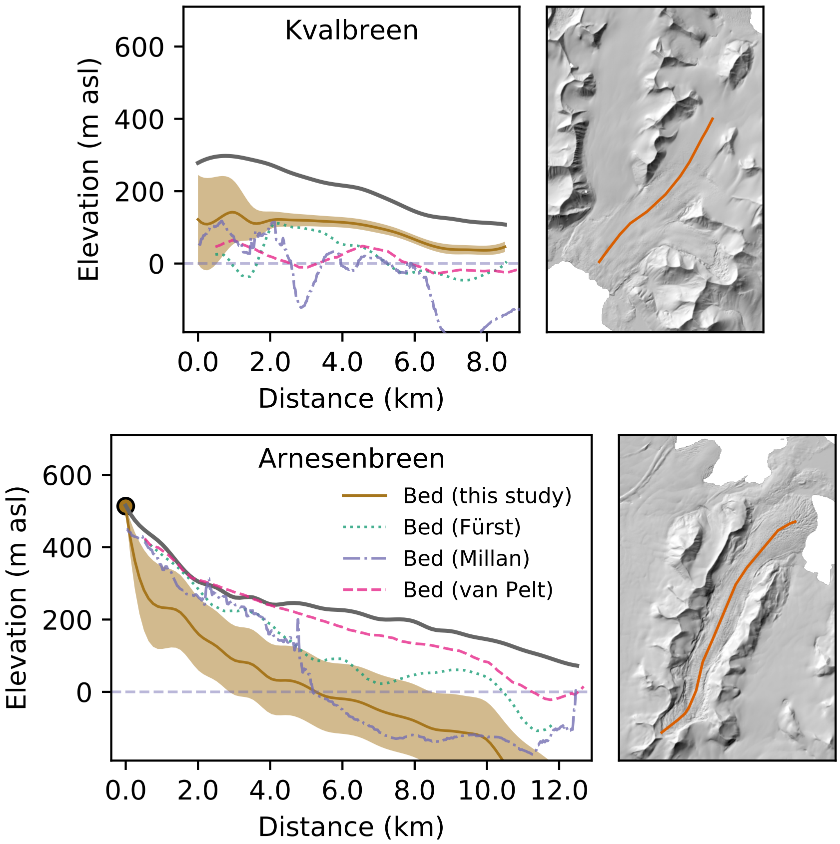

Figure 4.10.: Resulting surface and bed elevation (see caption Fig. 4.9).

caused a deflection of the ice flow towards the sides of the stagnant block at the terminus. Concluding, the models' one-dimensionality is not able to depict this behavior adequately.

4.3.5. Moršnevbreen

The surge of Moršnevbreen featured multiple years of delayed deceleration after the surge peak with still very high velocities. During this period, the entire glacier was taking part in the surge and was uniformly flowing towards the terminus. This flow regime holds the perfect conditions for the intended bed inference.

The results (Fig. 4.11) show a bed topography with comparatively low standard deviation. Unfortunately, no recent radar data is available which could provide information about the true ice thickness. However, the point at which the bed reaches sea level is

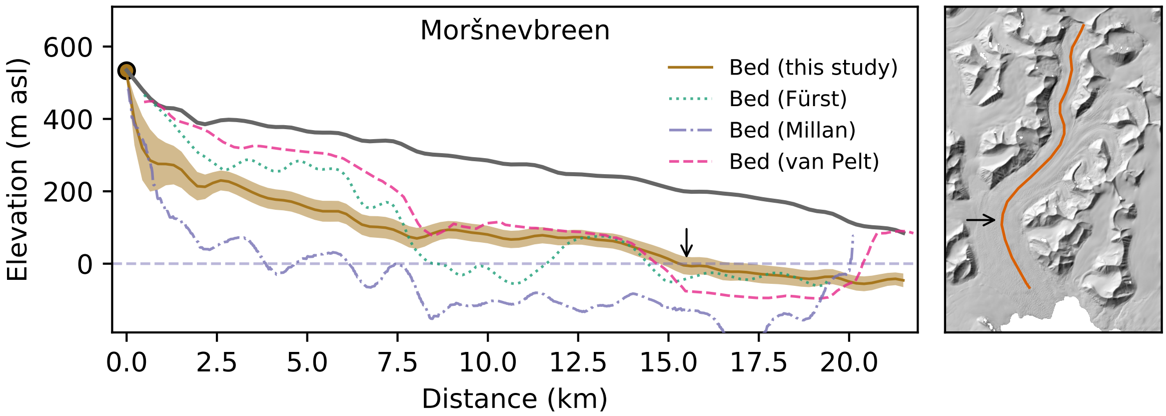

Figure 4.11.: Resulting surface and bed elevation (see caption Fig. 4.9).

indicated by an arrow and is in a realistic location. Also an elevation of 30–50 m below sea level close to the terminus is approximately in line with nautical charts (Kartverket, 2024).

5. Discussion

5.1. Glacier dynamics

Within the study area of Heer Land and a period from 2016 to 2024, a great number of glaciers can be found that exhibit surge-like behavior with an equally big variety of dynamics within this group.

In this study, different locations of surge initiation were found. A bulge starting in the upper glacier region and subsequently propagating down was observed on tidewater-terminating Moršnevbreen (Strongbreen system) and Nataschabreen (Paulabreen system), and also on land-terminating Vallåkrabreen and Scheelebreen. In the latter two cases, a sudden speedup was observed as the surge bulge reached the former terminus, followed by an advance. The sequence, involving a down-glacier propagation of a surge bulge from the glacier head, is the classical understanding of a surge, as described and categorized in three stages by Sund et al. (2009). While stage 1 and 2 are characterized by more or less gentle elevation changes, e.g., the bulge, only stage 3 shows typical signs of surging like intense speedup and crevassing.

Unlike Sund et al.'s suggestion for all surges, no bulges were observable preceding the surge of the tidewater-glaciers Kvalbreen and Arnesenbreen. On these glaciers, a clear surge front, initiated at the terminus, propagated upwards. A very similar behavior was found at other tidewater-surges in Svalbard by Sevestre et al. (2018). Here, a distinction was made between an initial slow phase with crevasses developing behind the front that is moving upwards and the following speedup. An identical development could be witnessed at Kvalbreen. Regarding this sequence in the framework of Sund's surge stages, only the real surge following the speedup shares characteristics with stage 3. An extended period of surge initiation can be observed but it does not share any characteristics with Sund's stage 1 or 2.

Another type of dynamics observable are the pronounced bulges on mostly small glaciers. Their motion and sometimes advance can last for decades and can lead to a surge-like mass redistribution. This behavior was observed on the small glaciers Bjuvbreen, Lognbreen, Klubbebreen and Fredbreen. Bjuvbreen was thoroughly studied by Hamilton (1992) who showed the presence and propagation of a bulge since 1977. Due to the rather low velocities, the glacier was interpreted to be in its quiescent phase. By now Bjuvbreen started advancing, still without dramatic increases in velocity. In other literature, similar events have been described as slow surge (Frappé and Clarke, 2007). Using the terminology of Sund et al., 2009, bulges are the first stage of a surge and hence these glaciers perform partial surges.

Summarizing the described dynamics, many glaciers experience a bulge preceding a surge. Tidewater glaciers can have this behavior, but can also exhibit upward crevasse-propagation without a bulge. Further, many mostly small glaciers experience bulging without ever speeding up in a (stage 3) surge fashion. This could suggest that bulge propagation and (stage 3) surging are somewhat separate phenomena which can but do not have to trigger each other.

5.2. Bed inference

The quality and uncertainty of the inferred bed topography varies strongly from glacier to glacier. While the glaciers with known or partially known bed topography suffered from obvious problems in the inversion and make a quantitative comparison pointless, other glaciers performed much better, producing seemingly realistic results. Generally, the application of the one-dimensional Bayesian model highlighted that the simplicity of this approach limits the trust in information about bed topography. However, even if the model itself struggles to produce sufficiently good output, the results can still be used to gain knowledge about bed inference on surging glaciers.

5.2.1. Bayesian model

The first obvious limitation of a one-dimensional model is the lack of results on basal topography off the flowline. Even if ice thicknesses could be interpolated within a known glacier outline, it is a clear advantage of two dimensional models to provide information about a whole glacier system.

Secondly, and more importantly, the flowline model is not informed about any lateral divergence or confluence of tributaries. This is taken care of by the flowline width which is adjusted during the Bayesian inference without observational constraints. Therefore, an ambiguity exists between the flowline width and the ice thickness. Some problems in the inversion results can be directly attributed to this ambiguity. For example, Scheelebreen and Arnesenbreen both are widening up close to their tidewater termini as the ice streams out of the more confined valley. In the model results this is noticeable as unrealistically high ice thicknesses while the flowline width remains approximately constant. Also in case of Vallåkrabreen the effects of confluent, fast flowing Firmbreen resulted in an unrealistic bed topography.

A future treatment of this issue could be the removal of the flowline width from the set of model parameters. Formulating the model for a whole flowband, with its width determined from the glacier outline, would allow for a pre-determined width parameter. Further, the introduction of a second dimension would solve the problem and could provide basal topography of the whole glacier.

The modeling approach demonstrated here was initially introduced as an interpolation scheme for sparse ice thickness observations (Brinkerhoff et al., 2016) and later adopted for bed inference studies (Morin et al., 2023). Therefore, the modeled bed topography should be treated with care due to the ambiguity discussed above. Also, in this study, the head and the terminus (land terminating) were treated as bed observations to constrain the glacier to its outline. In case of tidewater glaciers, a constraint at the terminus is not possible as the process of calving represents an unquantified flow of ice leaving the model domain. Running the model without a terminus bed constraint allowed application to tidewater glaciers and resulted in (partly) promising bed topographies (e.g., Scheelebreen). A further reduction of constraints was necessary for Kvalbreen which drains an almost stagnant ice cap of unknown thickness. Also in this case the model managed to produce a decent bed estimate. This behavior is what the used continuity equation (3.4) suggests as the ice thickness at a point on the flowline is only related to the integrated surface elevation change upstream of the point. Subsequently, no constraints are required apart from that no ice is entering the flowline from ahead.

5.2.2. Suitability of surges for bed inference

Before evaluating the posterior standard deviation, it is important to mention that this uncertainty is not necessarily a good indicator for the quality of the results because of systematic problems in the input data (velocity biases, Sec. 4.1). However, due to the applied Bayesian method, the bed standard deviation is an indicator for the magnitude of bed elevation variations that would produce observations close to the measurements. Hence, the standard deviation can give an idea about the amount of bed topography information contained in the observations.

Comparing the standard deviation of the posterior distributions among the different glaciers, strong variations can be observed. In Figure 5.1, the correlation between the uncertainty and the glacier surface velocity is shown. As visible, the bed standard deviation seems to be highly dependent on the surface velocity of the glacier during the period selected for the inversion. The found anticorrelation is remarkably strong, indicated by a Pearson correlation coefficient of $\rho = -0.99$. This, decrease in uncertainty in high velocity flow conditions confirms the importance of surges in bed inference studies with simple continuity-based models. These findings are in line with what Morin et al. (2023) showed previously for surging glaciers in North America.

Further, I was able to show the importance of selecting a well-suited period during a surge. Vallåkrabreen and Arnesenbreen were observed over longer periods during early

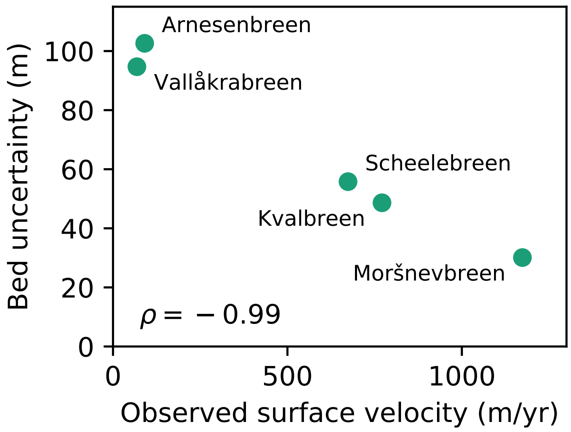

Figure 5.1.: Correlation between standard deviation of the resulting bed posterior and glacier velocity during the selected period with the associated pearson coefficient ρ. The mean velocity was computed by averaging over all velocities along the flowline. For the bed uncertainty, the mean posterior was subtracted from the posterior at all location along the flowline before the standard deviation was calculated.

and late stages of the surge (see time series in Fig. 4.2) with velocities much lower than their maximum surge speeds. This led to bed uncertainties more than three times higher than the ones from Moršnevbreen, whose observation window is fully inside a period of extremely high velocities. Also, the strong dependency on hyper-parameters in case of Vallåkrabreen, that was not found at Moršnevbreen indicates that in a regime of slow flow, significantly less information about the bed is carried in the data.

The narrow time frame of periods with suitable flow conditions puts high demands on the input data and especially their temporal coverage. As the velocity data used here shows significant gaps during most of the investigated surges, for some glaciers periods of slower flow were used. These two factors together seriously limited the quality of the results. Here, it should be mentioned that Morin et al. (2023) demonstrated the combination of data from multiple periods for one model run. This allows to avoid the manual selection of a suitable time window and is an important step towards automatization. However, the requirement for good input data during the optimal flow conditions of a surge remains.

5.2.3. Comparison with other bed topographies

During the recent years three studies aimed at modeling ice-free elevations or ice thicknesses in Svalbard. All basal topographies retrieved in these studies are shown along my results (Fig. 4.9 – 4.11).

Fürst et al. (2018) applied a two-dimensional mass conservation approach constrained by ice thickness radar data from a multitude of sources. For Heer Land exclusively airborne radar surveys from the 1980s from the Scott Polar Research Institute were assimilated. All glaciers discussed here were surveyed then and the data entered the bed topography presented by Fürst et al. The rest of the input data are from the years around 2010. The study did not implement any special treatment of active surges. Also, none of the glaciers interesting for this study surged around 2010. In case of Vallåkrabreen, of which the bed is known due to a recent ground penetrating radar survey (see Sec. 3.3), a significant difference between the true bed and Fürst et al. (2018) can be seen. While the latest radar survey shows an ice thickness of 200 m, Fürst et al. suggest around 100 m, based on the 80s radar. This suggests that quite big errors can be associated with the results from the 80s radar survey.

A global ice thickness product was presented by Millan et al. (2022). Here, a more simplistic approach that combines surface slope and surface velocity via a flow law was implemented. The data were acquired between 2017 and 2018 and therefore contains the surge of Moršnevbreen and early stages of the Arnesenbreen and Kvalbreen surge. The fact that the model is based on a simple flow law and that surges did not receive any special treatment leads to a drastic overestimation of ice thickness. At Arnesenbreen and Kvalbreen, even the position of the upward propagating surge front can be identified as a step between extremely low and reasonable ice thicknesses.

A few months before completion of this project, van Pelt and Frank, 2024 published a preprint of another glacier bed map of Svalbard explicitly treating surges different to other glaciers. Most glaciers were modeled using the Parallel Ice Sheet Model (PISM) or the Instructed Glacier Model (IGM) with datasets of surface velocity, surface elevation change, mass balance and more. Glaciers actively surging during the time of the velocity acquisition (2017-2018), namely Moršnevbreen, Arnesenbreen and others, were modeled with a simple perfect-plasticity model only influenced by surface slope. The reason for this separation was the temporal misalignment of the input data by a few years which is only relevant during the fast flow of a surge. Concluding, these surges were still not fully exploited but more excluded from the more sophisticated modeling as trouble makers. The previously mentioned radar data were used for calibrations only.

As Moršnevbreen is the only glacier with low uncertainty and without signs of potentially faulty results, a comparison to the mentioned other studies shall be made upon that glacier. The results from the present study, Fürst et al. and van Pelt and Frank generally agree with each other and show deviations only locally. Differences between these models lay in the range of 50–100 m. The ice thickness from Millan et al. is about twice as high as in the other studies, as the model did not account for the ongoing surge.

In the lower third of Moršnevbreen, the agreement between this study and Fürst et al. is high while in the middle part, van Pelt and Frank shows lower deviations from my result. Interestingly, in the upper third all other studies suggest a step in the bed topography where the flow line enters the main trunk from a tributary. The reason that this is not shown in the result of this study could be the previously discussed ambiguity between ice thickness and divergence. So it is likely that the model's one-dimensionality is not able to capture the full dynamics here.

6. Summary and outlook

In this project, the globally outstanding cluster of surging glaciers in Heer Land, Svalbard, was studied. Within a rather small area and only a few years of observations, I was able to find and describe a large variety of surges and surge-like behavior. Among the 15 glaciers with significant mass redistribution six qualified as surges (stage 3, Sund et al. (2009)) characterized by a sudden speedup, glacier-wide extension and heavy crevassing. While bulges, propagating downstream, occurred prior to most of these surges, two surges of tidewater glaciers were initiated at the terminus. Both ways of surge initiation were described before with evolutions matching the observed sequences very well. In both cases, a multi-year-long ramp up to a (stage 3) surge can be witnessed during the downward propagation of a bulge or the upward propagation of a surge front. Especially small glaciers often show a bulge driven advance without ever accelerating to a full surge (previously termed partial or slow surge). Subsequently, bulges and surges are often associated with each other, but also occurring separately.

When surges are utilized for bed inference, it is shown that the selection of a study period is crucial for the quality of the results. Even for periods of enhanced velocities during the initiation or termination of a surge, the variations in the flow regime can make the retrieval of a meaningful bed topography very hard. Best results were gained for periods after the peak velocities were reached but still remained on a high level. Then the glacier forms a uniform flow with maximum extension and a fully disintegrated surface. The glacier-wide mean velocity proved to be a good indication for the selection of a study period.

The continuity-based one-dimensional Bayesian model applied here, was able to highlight strengths and limitations of bed inference on surging glaciers. The findings of a bed inference pilot study that shows the potential of high-slip flow conditions (Morin et al., 2023) were confirmed. These results suggest that during a surge more information about bed topography is conveyed in velocity and elevation change data. Further, this study shows that in order to exploit continuity only a confined glacier head (without ice influx) but no constraint at the terminus is required, which allows application to tidewater glaciers without a complex quantification of calving. The main limitation of the used model is its one-dimensionality. Not only are the resulting bed elevations limited to a single flowline, but the model is also not informed about lateral divergence which makes the problem poorly constrained. For this reason, the use of similar but two-dimensional models is encouraged for future studies.

For the glaciers with meaningful results and low uncertainty, this study agrees well with other studies about the ice thicknesses in Svalbard, compared to the deviations between these previous studies. In the past, surges were treated as a troublemaker in bed inference. In contrast to that, the results of this study suggest a high potential of a continuity-based approach for gaining more information about the basal topography of surging glaciers.

Besides the model, the input data play a major role for the quality of the results and can limit the choice of a time window drastically. While ArcticDEM is providing a source of elevation data with very good temporal coverage, the choice of temporally dense velocities proved to be challenging. Here, the ITS_LIVE dataset was explored and found to be highly problematic. Even if no signs of wrong data were found, data gaps during a surge can lead to heavily biased mean velocities. In this study, tools to detect and mitigate these data gaps are presented. As shown here, it is necessary to use ITS_LIVE with care. In future studies the potential of other sources of velocity data could be explored (e.g., products derived from radar satellite imagery).

Acknowledgements

First, I want to thank my supervisors and examiners Christian Haas and Andy Hodson for making this work possible. It was the opportunity, they gave me that allowed my deep dive into the incredibly fascinating world of surging glaciers. As a consequence I was not only allowed to study these phenomena but I was able to live in Svalbard and to visit these glaciers on numerous field excursions. Further, I am thankful for the motivation Christian had for squeezing in my glacier surveys into the already packed schedule of Polar 5. Without their support and supervision I could not have developed my focus that strongly towards glaciology.

Further, I want to give great thanks to my third supervisor Erik Schytt Mannerfelt. He supported me throughout this project scientifically with endless ideas, his own motivation and expertise in very much everything I had to deal with. Besides Erik I also want to thank Ursula and Gabby for having such an amazing spring field season at the coolest surges in the world and for having all the discussions about the glaciers' intensions and characters.

Thanks should also go to Veit Helm who processed the collected flight data for me and to Adrian Luckman for providing me with some of his radar ice velocities.

Last but not least, I am extremely grateful to all my friends I met during my stay in Svalbard. With you it was possible to experience Svalbard and especially glaciers from a completely different perspective. All the crevasse, meltwater channel and ice cave adventures during all seasons only fueled my desire to understand glaciers. I gained endless personal experiences on hikes, ski and snowmobile trips, during our first whiteout,

in the cold of Svalbard and deep below the glacier surface. Without all the very special persons, living in midnight sun and polar night would not be worth it.

A. ALS flight planning

Additionally to ArcticDEM, for this study we collected elevation data from Vallåkrabreen and Scheelebreen in August 2023 with an airborne laser scanner (ALS). The research aircraft Polar 5 of type Basler BT-67 equipped with a RIEGEL VQ-580 laser scanner was used for the elevation measurements. The glaciers were covered in multiple overflights at an altitude of mainly 1000–1200 m above ground. While most of the tracks were flown at a constant altitude the central valley of the glaciers required climbing paths due to the significant variation in surface elevation along the paths. To ensure a full coverage in terms of field of view and maximum range, the scanner's swath was simulated on an existing DEM of the region while planning the flight tracks (see Fig. A.1). During the survey the glaciers were free of low clouds allowing for almost gap-free coverage.

From the distances recorded by the instrument, which are relative to the aircraft's position, the absolute georeferenced locations of data points can be computed from the on-board GPS receivers and position sensors. The processing was carried out by Veit Helm at the Alfred-Wegener-Institute in Bremerhaven. For a full description of the process see Helm, 2008.

Due to a lack of good velocity data from 2023 the full potential of the ALS data could not be exploited.

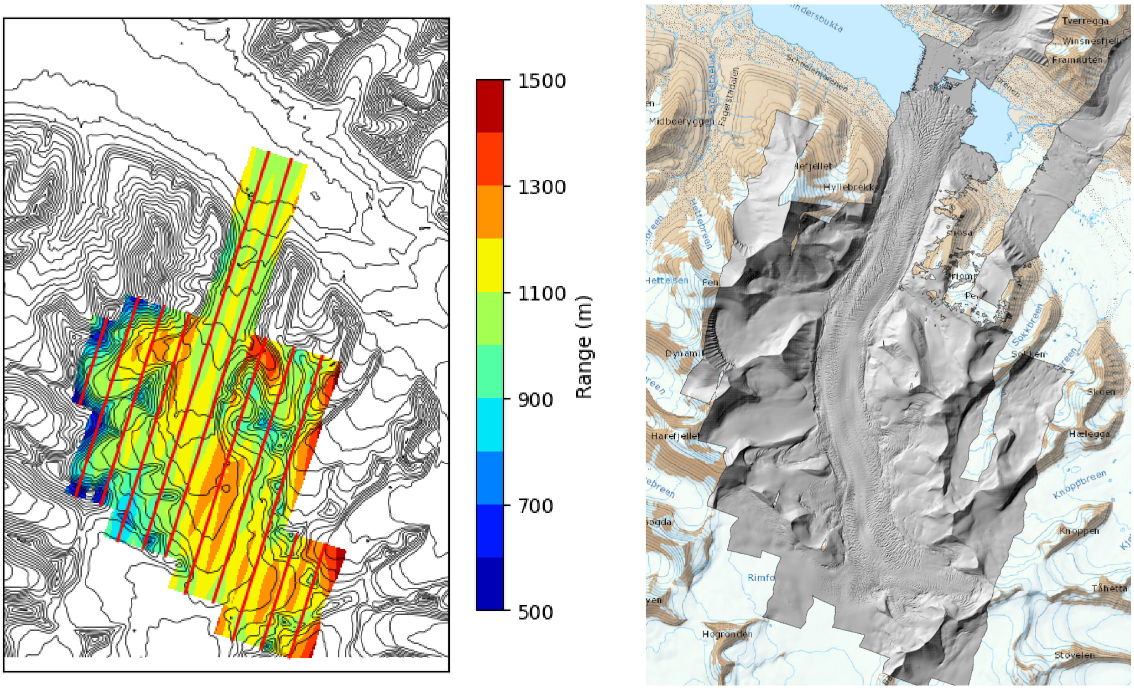

(a) Flight planning

(b) Resulting DEM

Figure A.1.: Planning and results of laser scanner survey flights for the example of Scheelebreen. During the planning, the altitude at the end points of each survey line (red) were chosen so that the individual stripes slightly overlap and that the maximum distance to the ground does not exceed the range of the laser scanner. Background right panel: Norwegian Polar Institute

B. Bayesian model output

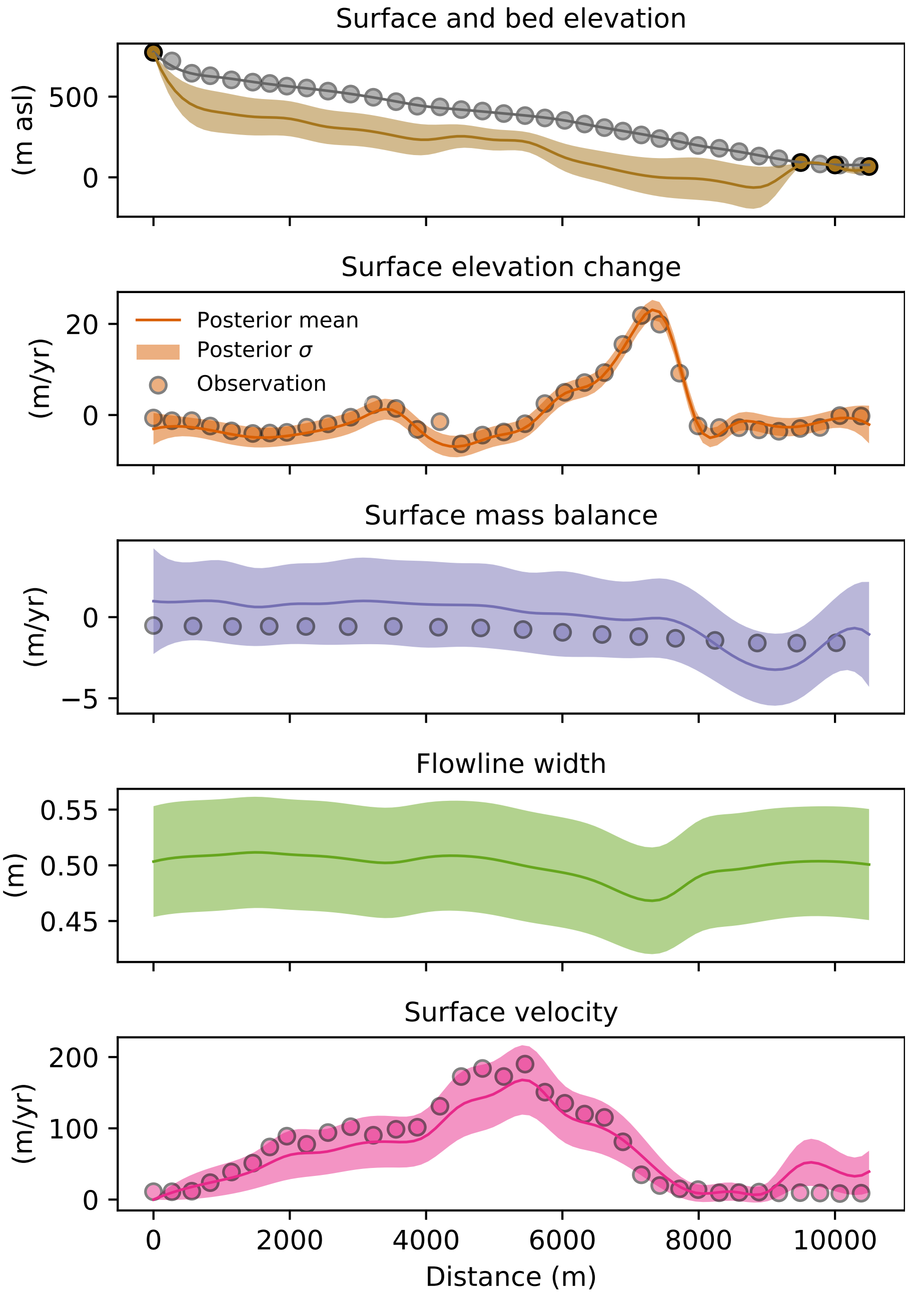

Figure B.1.: Bayesian model output for Vallåkrabreen.

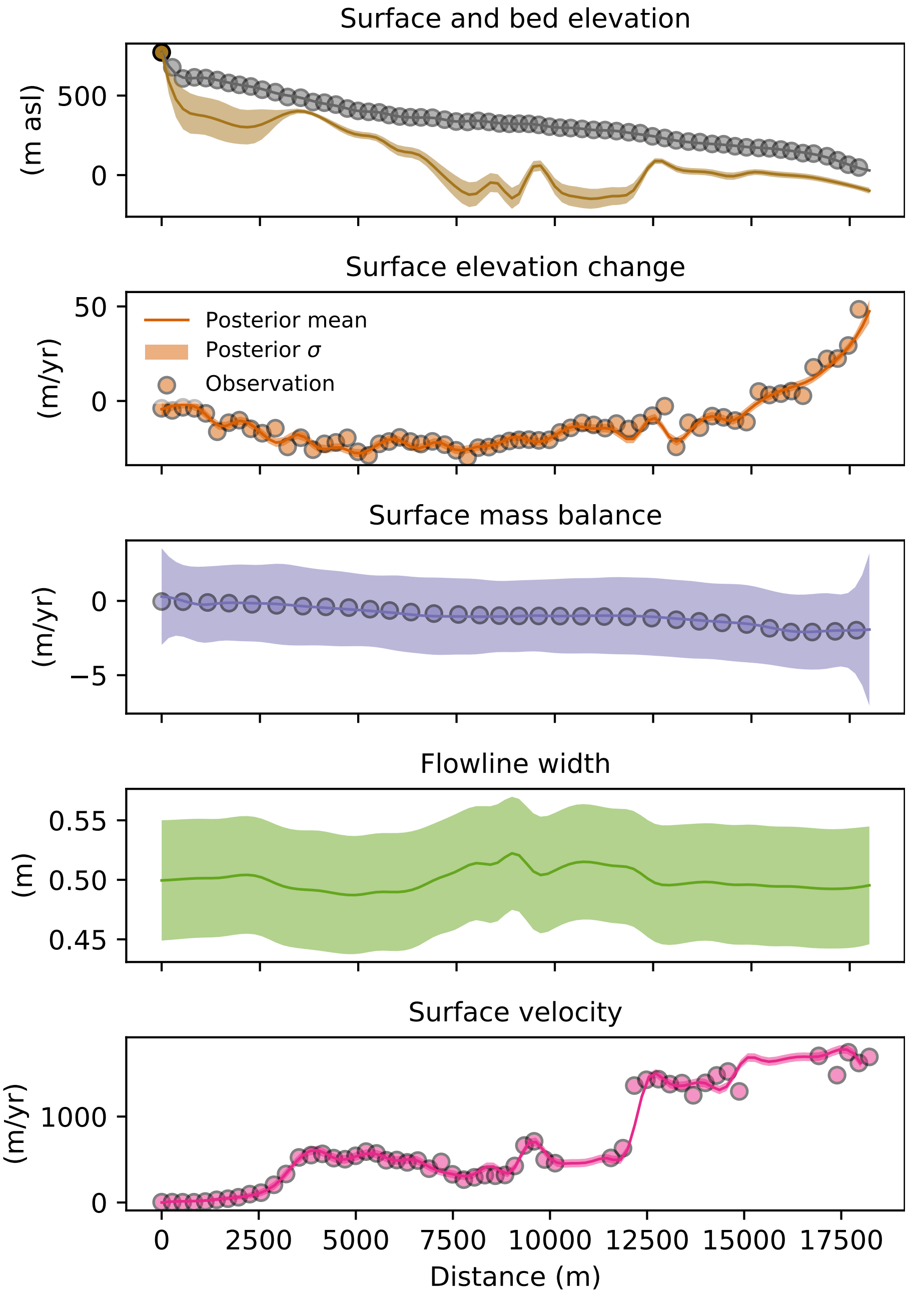

Figure B.2.: Bayesian model output for Scheelebreen.

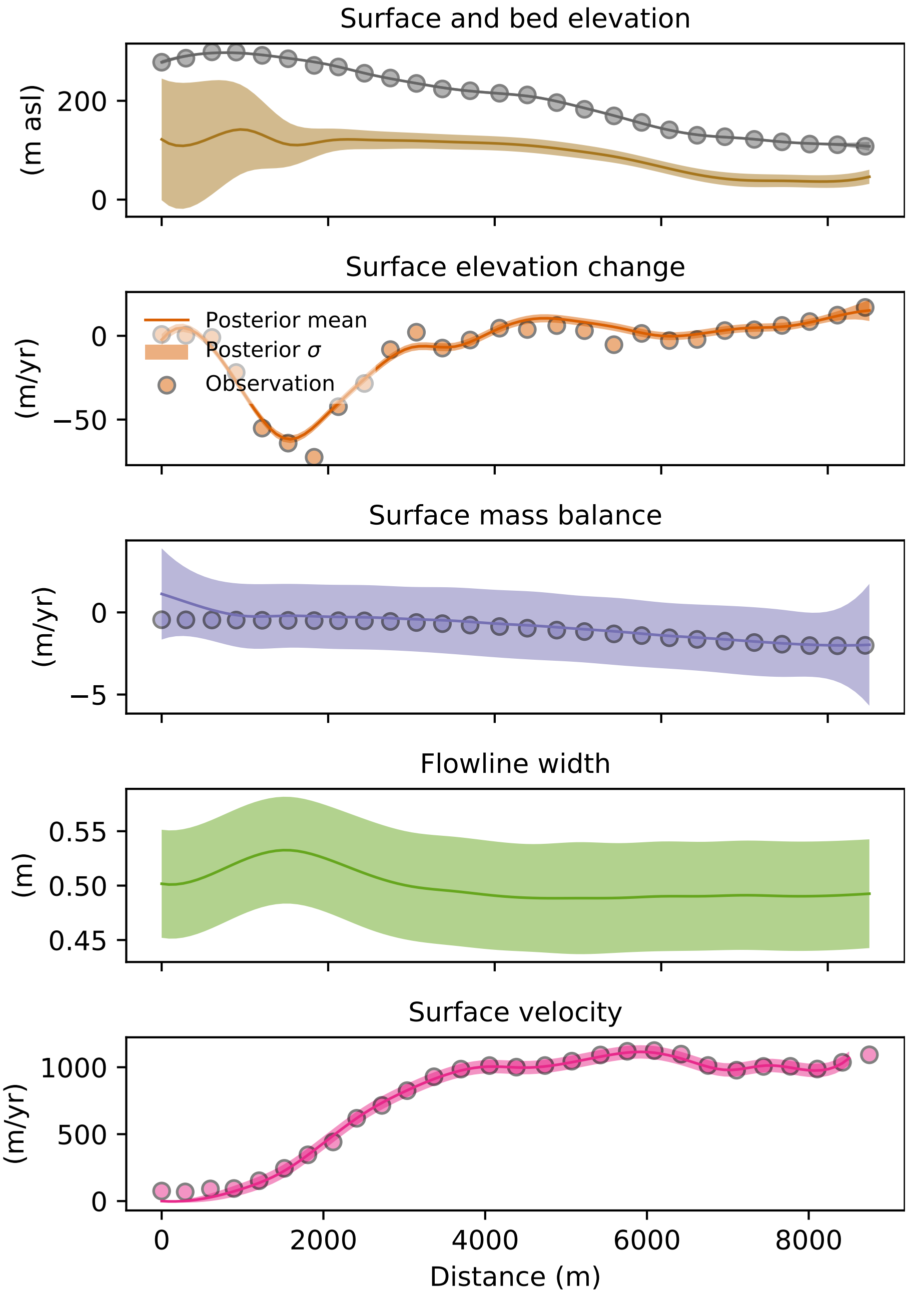

Figure B.3.: Bayesian model output for Kvalbreen.

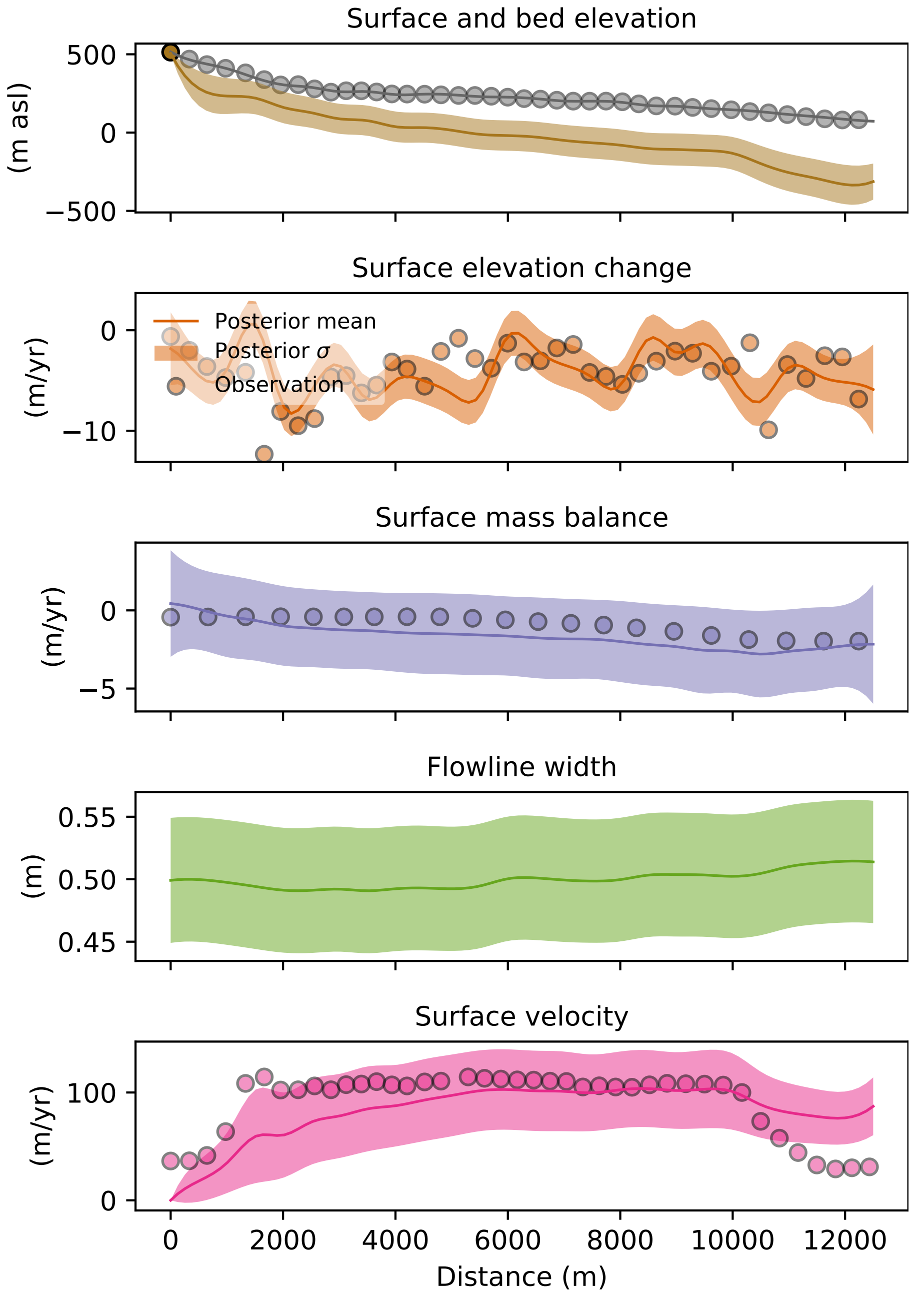

Figure B.4.: Bayesian model output for Arnesenbreen.

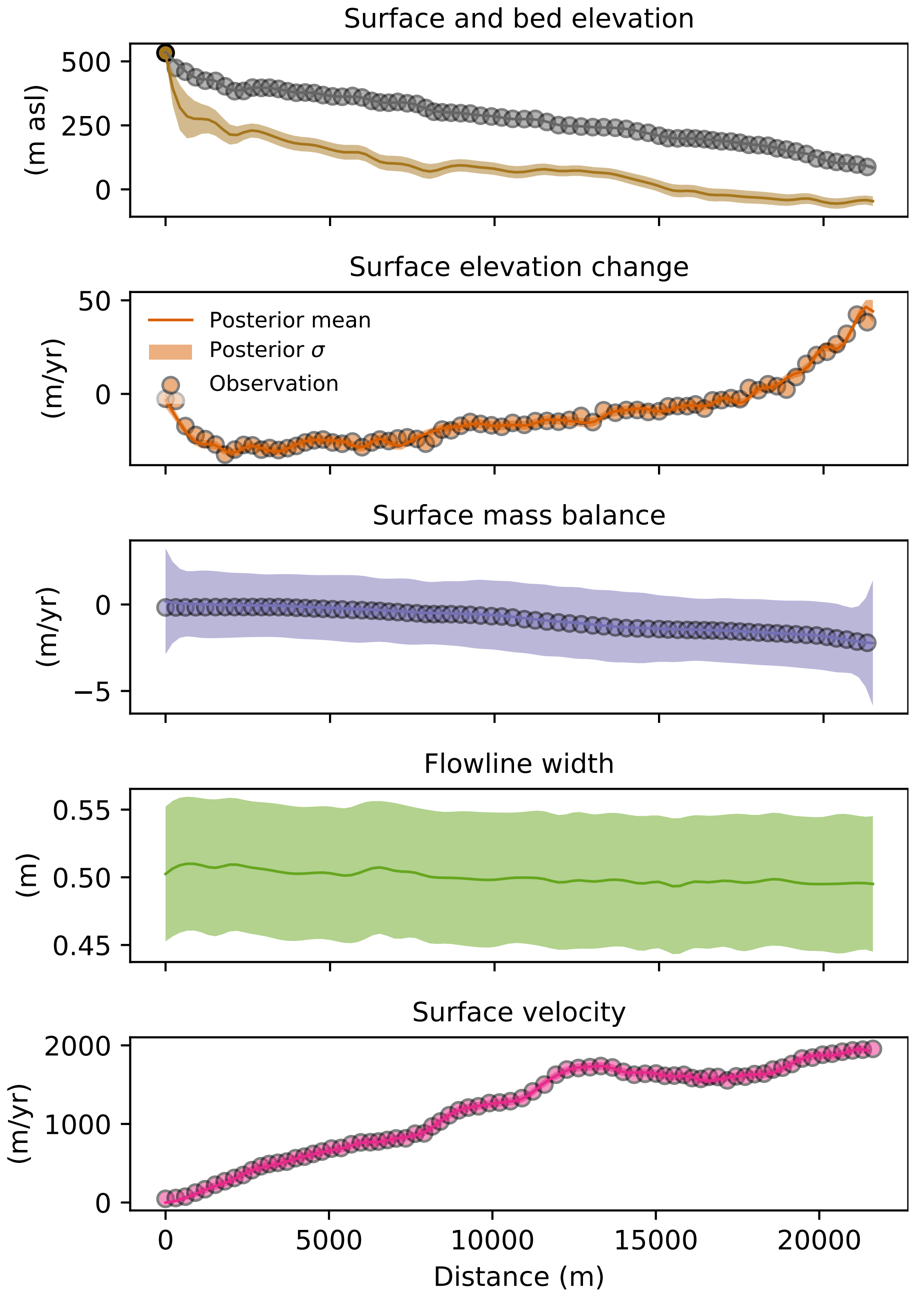

Figure B.5.: Bayesian model output for Moršnevbreen.

Bibliography

Abril-Pla, O., Andreani, V., Carroll, C., Dong, L., Fonnesbeck, C. J., Kochurov, M., Kumar, R., Lao, J., Luhmann, C. C., Martin, O. A., et al. (2023). PyMC: A modern, and comprehensive probabilistic programming framework in Python. *PeerJ Computer Science*, *9*, e1516.

Benn, D. I., & Evans, D. J. (2013). *Glaciers and glaciation*. Routledge.

Benn, D. I., Fowler, A. C., Hewitt, I., & Sevestre, H. (2019a). A general theory of glacier surges. *Journal of Glaciology*, *65*(253), 701–716. https://doi.org/10.1017/jog.2019.62

Benn, D. I., Jones, R. L., Luckman, A., Fürst, J. J., Hewitt, I., & Sommer, C. (2019b). Mass and enthalpy budget evolution during the surge of a polythermal glacier: A test of theory. *Journal of Glaciology*, *65*(253), 717–731. https://doi.org/10.1017/jog.2019.63

Besl, P. J., & McKay, N. D. (1992). Method for registration of 3-D shapes. In P. S. Schenker (Ed.), *Sensor fusion iv: Control paradigms and data structures* (pp. 586–606, Vol. 1611). SPIE. https://doi.org/10.1117/12.57955

Bouchayer, C., Aiken, J. M., Thøgersen, K., Renard, F., & Schuler, T. V. (2022). A machine learning framework to automate the classification of surge-type glaciers in Svalbard [e2022JF006597 2022JF006597]. *Journal of Geophysical Research: Earth Surface*, *127*(7), e2022JF006597. https://doi.org/https://doi.org/10.1029/2022JF006597

Brinkerhoff, D. J., Aschwanden, A., & Truffer, M. (2016). Bayesian inference of subglacial topography using mass conservation. *Frontiers in Earth Science*, *4*. https://doi.org/10.3389/feart.2016.00008

Clarke, G. K. C. (1976). Thermal regulation of glacier surging. *Journal of Glaciology*, *16*(74), 231–250. https://doi.org/10.3189/S0022143000031567

Clarke, G. K. C. (1991). Length, width and slope influences on glacier surging. *Journal of Glaciology*, *37*(126), 236–246. https://doi.org/10.3189/S0022143000007255

Clarke, G. K. C., Nitsan, U., & Paterson, W. S. B. (1977). Strain heating and creep instability in glaciers and ice sheets. *Reviews of Geophysics*, *15*(2), 235–247. https://doi.org/https://doi.org/10.1029/RG015i002p00235

Eisen, O., Harrison, W. D., & Raymond, C. F. (2001). The surges of Variegated Glacier, Alaska, U.S.A., and their connection to climate and mass balance. *Journal of Glaciology*, *47*(158), 351–358. https://doi.org/10.3189/172756501781832179

Fowler, A. C., & Johnson, C. (1996). Ice-sheet surging and ice-stream formation. *Annals of Glaciology*, *23*, 68–73. https://doi.org/10.3189/S0260305500013276

Frappé, T., & Clarke, G. K. C. (2007). Slow surge of Trapridge Glacier. *AGU Fall Meeting Abstracts*.

Fürst, J. J., Navarro, F., Gillet-Chaulet, F., Huss, M., Moholdt, G., Fettweis, X., Lang, C., Seehaus, T., Ai, S., Benham, T. J., Benn, D. I., Björnsson, H., Dowdeswell, J. A., Grabiec, M., Kohler, J., Lavrentiev, I., Lindbäck, K., Melvold, K., Pettersson, R., . . . Braun, M. H. (2018). The ice-free topography of Svalbard. *Geophysical Research Letters*, *45*(21), 11, 760–11, 769. https://doi.org/https://doi.org/10.1029/2018GL079734

Gardner, A., Fahnestock, M., & Scambos, T. (2022). MEaSUREs ITS_LIVE regional glacier and ice sheet surface velocities, version 1. https://doi.org/10.5067/6II6VW8LLWJ7

Gardner, A., Moholdt, G., Scambos, T., Fahnstock, M., Ligtenberg, S., van den Broeke, M., & Nilsson, J. (2018). Increased West Antarctic and unchanged East Antarctic ice discharge over the last 7 years. *The Cryosphere*, *12*(2), 521–547. https://doi.org/10.5194/tc-12-521-2018

Hamilton, G. S. (1992). Investigation of surge-type glaciers in Svalbard. https://doi.org/10.17863/CAM.27506

Hastings, W. K. (1970). Monte Carlo sampling methods using Markov chains and their applications. *Biometrika*, *57*(1), 97–109. Retrieved June 25, 2024, from http://www.jstor.org/stable/2334940

Helm, V. (2008). *Airborne SAR/Interferometric Radar Altimeter System (ASIRAS) - Kalibrierung, Validierung und Interpretation der Messergebnisse* [Dissertation]. Universität Bremen.

Herreid, S., & Truffer, M. (2016). Automated detection of unstable glacier flow and a spectrum of speedup behavior in the Alaska Range. *Journal of Geophysical Research: Earth Surface*, *121*(1), 64–81.

Huss, M. (2013). Density assumptions for converting geodetic glacier volume change to mass change. *The Cryosphere*, *7*(3), 877–887. https://doi.org/10.5194/tc-7-877-2013

Jiskoot, H., Murray, T., & Boyle, P. (2000). Controls on the distribution of surge-type glaciers in Svalbard. *Journal of Glaciology*, *46*(154), 412–422. https://doi.org/10.3189/172756500781833115

Kääb, A., Bazilova, V., Leclercq, P. W., Mannerfelt, E. S., & Strozzi, T. (2023). Global clustering of recent glacier surges from radar backscatter data, 2017–2022. *Journal of Glaciology*, *69*(277), 1515–1523. https://doi.org/10.1017/jog.2023.35

Kääb, A., Leinss, S., Gilbert, A., Bühler, Y., Gascoin, S., Evans, S. G., Bartelt, P., Berthier, E., Brun, F., Chao, W.-A., et al. (2018). Massive collapse of two glaciers in western Tibet in 2016 after surge-like instability. *Nature Geoscience*, *11*(2), 114–120.

Kamb, B., Raymond, C. F., Harrison, W. D., Engelhardt, H., Echelmeyer, K. A., Humphrey, N., Brugman, M. M., & Pfeffer, T. (1985). Glacier surge mechanism: 1982-1983 surge of Variegated Glacier, Alaska. *Science*, *227*(4686), 469–479. https://doi.org/10.1126/science.227.4686.469

Kartverket. (2024). Sjøkart [Accessed July, 2024]. norgeskart.no

Kienholz, C., Rich, J. L., Arendt, A. A., & Hock, R. (2014). A new method for deriving glacier centerlines applied to glaciers in [alaska] and northwest Canada. *The Cryosphere*, *8*(2), 503–519. https://doi.org/10.5194/tc-8-503-2014

Lovell, H., & Fleming, E. J. (2023). Structural evolution during a surge in the Paulabreen glacier system, Svalbard. *Journal of Glaciology*, *69*(273), 141–152.

Luckman, A., Murray, T., Jiskoot, H., Pritchard, H., & Strozzi, T. (2003). ERS SAR feature-tracking measurement of outlet glacier velocities on a regional scale in East Greenland. *Annals of Glaciology*, *36*, 129–134. https://doi.org/10.3189/172756403781816428

Mannerfelt, E. S. (2023a). Adsvalbard. *GitHub repository*. https://github.com/erikmannerfelt/ADSvalbard

Mannerfelt, E. S. (2023b). Rsgpr. *GitHub repository*. https://github.com/erikmannerfelt/rsgpr

Meier, M. F., & Post, A. (1969). What are glacier surges? *Canadian Journal of Earth Sciences*, *6*(4), 807–817. https://doi.org/10.1139/e69-081

Millan, R., Mouginot, J., Rabatel, A., & Morlighem, M. (2022). Ice velocity and thickness of the world's glaciers. *Nature Geoscience*, *15*(2), 124–129. https://doi.org/10.1038/s41561-021-00885-z

Morin, A., Flowers, G. E., Nolan, A., Brinkerhoff, D., & Berthier, E. (2023). Exploiting high-slip flow regimes to improve inference of glacier bed topography. *Journal of Glaciology*, *69*(275), 658–664. https://doi.org/10.1017/jog.2022.121

Murray, T., Dowdeswell, J. A., Drewry, D. J., & Frearson, I. (1998). Geometric evolution and ice dynamics during a surge of Bakaninbreen, Svalbard. *Journal of Glaciology*, *44*(147), 263–272. https://doi.org/10.3189/S0022143000002604

Murray, T., Luckman, A., Strozzi, T., & Nuttall, A.-M. (2003). The initiation of glacier surging at Fridtjovbreen, Svalbard. *Annals of Glaciology*, *36*, 110–116. https://doi.org/10.3189/172756403781816275

Murray, T., Stuart, G. W., Miller, P. J., Woodward, J., Smith, A. M., Porter, P. R., & Jiskoot, H. (2000). Glacier surge propagation by thermal evolution at the bed. *Journal of Geophysical Research: Solid Earth*, *105*(B6), 13491–13507. https://doi.org/https://doi.org/10.1029/2000JB900066

Nuth, C., & Kääb, A. (2011). Co-registration and bias corrections of satellite elevation data sets for quantifying glacier thickness change. *The Cryosphere*, *5*(1), 271–290. https://doi.org/10.5194/tc-5-271-2011

Paul, F., Piermattei, L., Treichler, D., Gilbert, L., Girod, L., Kääb, A., Libert, L., Nagler, T., Strozzi, T., & Wuite, J. (2022). Three different glacier surges at a spot: What satellites observe and what not. *The Cryosphere*, *16*(6), 2505–2526. https://doi.org/10.5194/tc-16-2505-2022

Petrenko, V. F., & Whitworth, R. W. (1999). *Physics of ice*. OUP Oxford.

Porter, C., Howat, I., Noh, M.-J., Husby, E., Khuvis, S., Danish, E., Tomko, K., Gardiner, J., Negrete, A., Yadav, B., Klassen, J., Kelleher, C., Cloutier, M., Bakker, J., Enos, J., Arnold, G., Bauer, G., & Morin, P. (2022). *ArcticDEM - Strips, Version 4.1*. https://doi.org/10.7910/DVN/C98DVS

RGI 7.0 Consortium. (2023). Randolph Glacier Inventory - A dataset of global glacier outlines, version 7.0. https://doi.org/10.5067/f6jmovy5navz

Schmidt, L. S. (2022). CryoGrid simulations of Svalbard mass balance, refreezing and runoff, 1991-2022. https://doi.org/10.21343/NCWC-S086

Sevestre, H., & Benn, D. I. (2015). Climatic and geometric controls on the global distribution of surge-type glaciers: Implications for a unifying model of surging. *Journal of Glaciology*, *61*(228), 646–662. https://doi.org/10.3189/2015JoG14J136

Sevestre, H., Benn, D. I., Hulton, N. R. J., & Bælum, K. (2015). Thermal structure of Svalbard glaciers and implications for thermal switch models of glacier surging.

Journal of Geophysical Research: Earth Surface, *120*(10), 2220–2236. https://doi.org/https://doi.org/10.1002/2015JF003517

Sevestre, H., Benn, D. I., Luckman, A., Nuth, C., Kohler, J., Lindbäck, K., & Pettersson, R. (2018). Tidewater glacier surges initiated at the terminus. *Journal of Geophysical Research: Earth Surface*, *123*(5), 1035–1051. https://doi.org/https://doi.org/10.1029/2017JF004358

Sund, M. (2006). A surge of Skobreen, Svalbard. *Polar Research*, *25*(2), 115–122.

Sund, M., Eiken, T., Hagen, J. O., & Kääb, A. (2009). Svalbard surge dynamics derived from geometric changes. *Annals of Glaciology*, *50*(52), 50–60. https://doi.org/10.3189/172756409789624265

van Pelt, W., & Frank, T. (2024). A new glacier thickness and bed map for Svalbard. *EGUsphere*, *2024*, 1–22. https://doi.org/10.5194/egusphere-2024-1525